# Early loss of endogenous $NAD^+$ following rotenone treatment leads to Sarm1 activation that is ameliorated by PARP inhibition

Ankita Sarkar[1], Malinki Sur[1], Sourav Dutta[1], Puja Dey[1] and Piyali Mukherjee[1,*]

[1]School of Biotechnology, Presidency University

Canal Bank Rd, DG Block, Action Area 1D, New Town,

Kolkata-700156, West Bengal, India, Tel: +91 8017086495

* Corresponding author email: piyali.dbs@presiuniv.ac.in

Running title: PARP inhibition reverses rotenone-induced cell death

**Key words:** $NAD^+$, Sarm1, Rotenone, PARP inhibitor, PJ34, Mitochondria, Autophagy

**Abstract**

Sarm1 is an evolutionary conserved innate immune adaptor protein that has emerged as a primary regulator of programmed axonal degeneration over the past decade. *In vitro* structural insights have revealed that although Sarm1 induces energy depletion by breaking down $NAD^+$, it is also allosterically inhibited by $NAD^+$. However, how $NAD^+$ levels modulate the activation of intracellular Sarm1 has not been elucidated so far. This study focuses on understanding the events leading to Sarm1 activation in both neuronal and non-neuronal cells using the mitochondrial complex I inhibitor rotenone. Here we report the regulation of rotenone-induced cell death by loss of $NAD^+$ that may act as a "biological trigger" of Sarm1 activation. Our study revealed that early loss of endogenous $NAD^+$ levels arising due to PARP1 hyperactivation preceded Sarm1 induction following rotenone treatment. Interestingly, replenishing $NAD^+$ levels by the PARP1 inhibitor, PJ34 restored mitochondrial homeostasis and prevented subsequent Sarm1 activation in rotenone treated cells. These cellular data were further validated in *Drosophila melanogaster* where a significant reduction in rotenone mediated loss of locomotor abilities and reduced dSarm expression was observed in the flies following PARP inhibition. Taken together, these observations not only uncovers a novel regulation of Sarm1 induction by endogenous $NAD^+$ levels but also point towards an important understanding on how PARP inhibitors could be repurposed in the treatment of mitochondrial complex I deficiency disorders mediated by Sarm1.

36 **Introduction**

37 Mitochondrial complex I deficiency has been reported in a number of diseases with
38 mitochondrial disorders and has been strongly linked to patients with Parkinson's disease (PD)
39 [1,2]. Rotenone, a lipophilic insecticide, has been shown to be a potent inhibitor of
40 mitochondrial complex I [3,4]. Several studies have indicated that rotenone mediated cell death
41 is associated with mitochondrial depolarization, DNA damage and ROS formation that
42 corroborates with similar observation in other mitochondrial complex I deficiency disorders [5,
43 6,7,8]. So, how this mitochondrial dysfunction induced by rotenone correlates with cell death?
44 Our previous study has indicated that the TLR adaptor protein sterile alpha and TIR motif
45 containing 1 (Sarm1) plays a pivotal role in this process as Sarm1 knockdown showed a
46 significant reduction in rotenone induced cell death in SH-SY5Y cells [9]. Further, a study by
47 *Hughes et al* has revealed that Sarm1 inhibition can prevent axonal degeneration following
48 rotenone treatment [10]. Sarm1 is a $NAD^+$-hydrolyzing enzyme that upon activation results in
49 loss of nicotinamide adenine dinucleotide$^+$ ($NAD^+$) resulting in severe energy depletion within
50 the axons with subsequent induction of axonal degeneration [11,12,13]. Although Sarm1 has
51 emerged as an important regulator of programmed axonal destruction, how the expression and
52 activation of endogenous Sarm1 is regulated within the cell is not well defined till date. Further,
53 the non-neuronal regulation of this protein is understudied although this protein has been
54 shown to be expressed in the liver, kidney and immune cells [14]. Since Sarm1 and rotenone
55 induced cell death seems to be intricately linked, we envisioned that this may serve as an
56 excellent cellular model to understand how this protein is endogenously regulated during

57 mitochondrial complex I deficiency disorders and whether a single event or a cumulative
58 phenomenon acted as a biological trigger of Sarm1 activation within the cells.

59 Although Sarm1 has been shown to mediate rotenone induced cell death, it is not
60 known how $NAD^+$ levels modulates this process. Recent reports indicated that $NAD^+$ acts as a
61 key determinant of mitochondrial health and homeostasis [15,16] and decides cell fate by
62 participating in cell death networks like apoptosis, autophagy or parthanatos [17,18,19]. Under
63 situations of stress that induces mitochondrial damage, a process termed 'mitophagy' is
64 initiated to remove these damaged organelles and restore cellular homeostasis. It has been
65 suggested that upon various cellular stresses accumulation of damaged mitochondria arising
66 due to incomplete clearance by mitophagy is associated with rapid cell death in the absence of
67 a functional autophagy machinery [20]. Studies on rotenone mediated autophagy are
68 inconclusive [21] and it is unclear whether defective mitochondrial clearance by mitophagy
69 plays a determining role in rotenone induced cell death. Further, how $NAD^+$ status affects the
70 overall bioenergetic balance within the cells that may drive key cellular processes like
71 autophagy and apoptosis is not clearly defined.

72 The two main classes of enzymes that are responsible for maintaining intracellular $NAD^+$
73 pool are the $NAD^+$ consuming enzymes Sirtuins and PARPs [22,23,24]. While the short-term
74 activation of PARPs triggering a DNA damage response is considered to be crucial for
75 maintaining cellular homeostasis, prolonged activation of PARPs leads to rapid degradation of
76 $NAD^+$ and eventually cell death [25,26]. Interestingly, rotenone induced oxidative DNA damage
77 has been reported in a few studies with Parkinson's disease (PD) patient samples [27,28] that
78 could lead to PARP1 hyperactivation and loss of $NAD^+$ following rotenone treatment.

79 We report here that rotenone induced temporal regulation of $NAD^+$ levels lead to a
80 sequential triggering of events that ultimately cause cell death. Our study indicates that
81 rotenone treatment results in an early loss of $NAD^+$ that is accompanied by mitochondrial
82 dysfunction and PARP1 hyperactivation that may serve as the "biological trigger" of Sarm1
83 induction which has been previously shown to be allosterically inhibited by $NAD^+$ using *in vitro*
84 systems [29,30,31]. In concurrence with these observations, replenishing $NAD^+$ levels by pre-
85 incubation of cells with the PARP inhibitor PJ34 or Olaparib restored cellular $NAD^+$ levels,
86 prevented Sarm1 activation and significantly reduced cell death following rotenone treatment.
87 To obtain a generalized overview of rotenone-mediated $NAD^+$ regulation and Sarm1 activation,
88 we conducted our studies in both non-neuronal and neuronal cell lines HEK293 and SH-SY5Y,
89 respectively. To strengthen our hypothesis, we extended our findings in a previously
90 established rotenone model of Drosophila and our results showed reversal of rotenone-induced
91 locomotor deficits in the presence of the PARP inhibitor Olaparib in the flies. Thus, results
92 generated from this study not only provides the first evidence of regulation of Sarm1
93 expression by endogenous $NAD^+$ levels but also offers the exciting opportunity of repurposing
94 PARP inhibitors in the treatment of Sarm1-induced pathological conditions and mitochondrial
95 complex I deficiency disorders.
96
97 **Results**
98 **Rotenone induced cell death in both non-neuronal and neuronal cells that was independent**
99 **of caspase-3 activation**

100 Mitochondrial complex I is the first point of entry of electrons to the electron transport
101 chain and its inhibition has been implicated in different pathological conditions like PD [32].
102 Here we attempted to gain a comprehensive mechanistic insight in rotenone-mediated cell
103 death in the routinely used non neuronal cell line HEK293 and the neuronal cell line SH-SY5Y.
104 Our results indicate that rotenone induced cell death in a dose and time-dependent manner in
105 both HEK293 and SH-SY5Y cells (Fig. 1 A and B). We observed that in HEK293 cells almost 40%
106 cell death was achieved at a dose as low as 500 nM in 24 h. In comparison to the HEK293 cells, ,
107 a dose of 5 μM could induce a comparable cell death phenomenon in the neuronal cell line SH-
108 SY5Y, at 24 h (Fig. 1B) that also led to retraction of the cellular processes at 24 h post treatment
109 (Fig. 1C). Due to its greater susceptibility to mitochondrial complex I inhibition, we further
110 evaluated the status of apoptosis in HEK293 cells following rotenone treatment. Rotenone
111 treatment in HEK293 cells resulted in caspase-3 activation as indicated by increased
112 accumulation of active caspase-3 in the cells treated with 500 nM of rotenone (Fig. 1D).
113 However, contrary to our expectation, prior incubation with the PAN caspase inhibitor Z-VAD-
114 FMK followed by rotenone treatment did not reverse rotenone-induced cell death in both
115 HEK293 and SH-SY5Y cells (Fig. 1E) indicating that caspase activation was perhaps not the sole
116 factor driving rotenone induced cell death. This prompted us to perform an in-depth analysis of
117 the underlying mechanism leading to rotenone induced cell death using both non-neuronal
118 HEK293 cells and the neuronal SH-SY5Y cells.
119
120 **Rotenone induced cell death is accompanied by early mitochondrial dysfunction, increased**
121 **ROS accumulation and defective autophagy**

122 Cytochrome c released from damaged or leaky mitochondria stimulates the cleavage of
123 caspase-3 to its active form [33]. Since we observed caspase-3 activation we undertook a
124 detailed analysis of mitochondrial status following rotenone treatment. Our results in HEK293
125 cells show mitochondrial membrane depolarization in these cells as early as 4 h post-rotenone
126 treatment that preceded cell death as observed by staining with the cell permeant dye, TMRM
127 that accumulates only in active mitochondria (Fig. 2A). A similar phenomenon was also
128 observed in SH-SY5Y cells at 4 h post-treatment with 5 μM of rotenone (Fig. 2B). Further, live
129 staining with mitotracker green (that localizes to the mitochondria irrespective of mitochondrial
130 membrane potential) showed significant loss in mitochondrial puncta structure (as indicated by
131 arrows in the enlarged panel) in rotenone treated SH-SY5Y cells (Fig. 2C) as well as in HEK293
132 cells (Fig. 2D) but the mitochondria stained brighter compared to untreated controls which
133 could be indicative of accumulation of damaged mitochondria in these cells. It is well
134 established that mitochondrial damage leads to increased ROS production [7] and accumulating
135 ROS level causes further mitochondrial damage that may perpetuate ROS production in
136 rotenone treated cells. Rotenone has been shown to induce cellular ROS generation but the
137 source of this ROS is not well defined in HEK293 cells. To understand the source of ROS in these
138 cells, we analyzed the status of mitochondrial ROS and observed an increase in mitochondrial
139 ROS levels as indicated by increased Mitosox staining (Fig. 2E) as early as 4 h post-treatment.
140 Conforming to previous reports, we observed an increase in total ROS levels in rotenone
141 treated HEK293 (Fig. 2F) in a time-dependent manner and prior incubation with the anti-
142 oxidant NAC significantly ($P < 0.001$) reduced ROS generation both at 6 and 24 h post treatment
143 (Fig. 2F) in these cells. Interestingly, although there was heightened ROS production following

144 rotenone treatment, prior incubation with NAC did not significantly (P value 0.1) reverse the
145 ongoing cell death process in both HEK293 cells (Fig. 2G) as well as SH-SY5Y cells (Fig. 2H).
146 Taken together, these data indicated that heightened ROS production may be the effect of
147 accumulation of damaged mitochondria and may trigger a sequence of events that cannot be
148 abrogated by prior treatment with NAC. It is interesting to note here that although
149 mitochondrial dysfunction was observed as early as 4 h post rotenone treatment, apoptosis
150 was not induced at this time point as no AIF accumulation was observed within the nucleus at 4
151 h post-treatment (Fig. 2I)

152 Accumulation of damaged mitochondria that resulted in increased ROS production
153 could be due to a defective mitochondrial turnover via autophagy. Therefore, to correlate
154 mitochondrial dysfunction and increased ROS production in HEK293 cells, we were inclined to
155 check the status of autophagy in these cells. Microtubule-associated protein 1 light chain 3B
156 (LC3B) and p62/sequestosome 1 are two widely used autophagy markers [34,35]. Our results
157 showed an increase in p62 accumulation (an indicator of defective autophagic flux) in rotenone
158 treated HEK293 cells as well as SH-SY5Y cells as early as 4 h post-treatment (Fig. 2J and K). Co-
159 staining with endogenous LC3B showed higher nuclear LC3B staining in rotenone treated
160 HEK293 cells as compared to the control cells indicated by arrows (Fig. 2J right panel). Further,
161 co-staining with mitotracker green and lysotracker red did not reveal any co-localization in
162 rotenone treated cells at 4 h post-treatment (Fig. 2L) which indicated that mitophagy was not
163 initiated in these cells at this earlier time point. We next sought to understand whether p62
164 accumulation following rotenone treatment was due to decreased autophagosome-lysosome
165 fusion or defect in autophagic flux. For this, cells were transfected with the mCherry-GFP-LC3

166 plasmid and since GFP signal is lost under the acidic environment of the lysosome, the mCherry
167 positive cells confirms a functional autophagic flux within the cells [35,36]. Transfection with
168 mCherry-GFP-LC3 showed increased accumulation of yellow puncta in rotenone treated cells as
169 opposed to the red puncta (Fig. 2M) indicating it is not the autophagosome formation but a
170 defect in autophagic flux that could result in limited turnover of damaged mitochondria in
171 rotenone treated cells. Real time analysis of key autophagy genes revealed several fold higher
172 inductions of the Atg genes (Fig. S1A-C) as compared to the DMSO treated control cells but
173 reduced expression of a few late autophagy genes like Ulk1 (unc-51-like kinase 1) that plays an
174 important role in the formation of autophagosome at both early and late time points following
175 rotenone treatment in HEK293 (Fig. S1A) and SH-SY5Y cells (Fig. S2B-C).
176

177 **Rotenone treatment resulted in depletion of cellular $NAD^+$ levels and PARP inhibition by PJ34**
178 **prevented rotenone-induced cell death in both HEK293 and SH-SY5Y cells**

179 Since rotenone-induced autophagy did not go to completion, we asked whether energy
180 deficits within the cells prevented autophagic degradation of damaged mitochondria via the
181 lysosomal pathway. Accumulating recent evidence indicates that cellular $NAD^+$ homeostasis is
182 intricately associated with functional autophagy [37,38] which helps the cells further to adapt
183 to energy deprivation by obtaining energy from autophagic degradation products. Here we
184 speculated whether the $NAD^+$-consuming enzymes of the cells like PARP1 and Sirt1 have any
185 role in autophagic defect that may lead to increased accumulation of damaged mitochondria
186 and drive rotenone mediated cell death. Our results suggested that rotenone treatment
187 reduced $NAD^+$/NADH ratio thus decreasing total cellular $NAD^+$ levels in HEK293 cells at 24 h post

188 rotenone treatment (Fig. 3A). Interestingly, prior incubation of cells with the PARP1 inhibitor
189 PJ34 significantly (P<0.001) reversed rotenone induced cell death in HEK293 cells (Fig. 3B). To
190 further confirm the importance of $NAD^+$ replenishment in the reversal of rotenone induced cell
191 death, we analyzed the role of PJ34 in the neuronal cell line SH-SY5Y and a significant (P<0.001)
192 restoration of cell death following prior incubation with PJ34 was also observed in these cells
193 (Fig. 3C). However, a dose dependent analysis revealed that a higher does (50–100 μM) of PJ34
194 was required to achieve this reversal as compared to 25 μM in HEK293 cells. There was also a
195 differential expression pattern of the genes involved in $NAD^+$ metabolism pathway especially
196 that of *Nmnat1* and *Nmnat2* (key enzymes implicated in the regulation of the NADase Sarm1
197 mediated axonal degeneration) in rotenone treated HEK293 cells (Fig. S2A-D). Notably, loss of
198 $NAD^+$ was observed as early as 2 h in rotenone treated HEK293 cells (Fig. 3) and pre-incubation
199 of these cells with PJ34 followed by rotenone treatment restored cellular $NAD^+$ levels at 4 h
200 post treatment indicating that early drop in $NAD^+$ levels was a key player in rotenone induced
201 cell death. In comparison to the PARP inhibitor, the Sirtuin1 inhibitor EX527 had no such effect
202 on rotenone mediated cell death (Fig. 3E) in HEK293 cells. To understand whether PJ34 had a
203 similar effect on other inhibitors of the mitochondrial OXPHOS system, HEK293 cells were
204 treated with the mitochondrial complex III and V inhibitor Antimycin and Oligomycin
205 respectively which revealed that PJ34 had no effect in the reversal of cell death induced by
206 these inhibitors (Fig. S2 E-F) and was specific to the complex I inhibitor rotenone.

207 PARP is a DNA damage sensor and it has recently been shown that there is increased
208 localization of PARP1 to H2AX.2 enriched chromatin damage sites [39] and phosphorylated
209 H2AX.2 is a histone marker of DNA double strand breaks [40]. Our results showed that there

210 was increased level of phosphorylated H2AX (p-Ser 139) in the presence of rotenone, the level
211 of which is significantly decreased following pre-incubation with PJ34 and subsequent rotenone
212 treatment (Fig. 3F). This reduction in DNA damage alongwith the reversal mediated by PJ34
213 suggested that reduction of PARP hyperactivity in the presence of rotenone may prevent early
214 $NAD^+$ loss thus reducing cellular energy deficits. Additionally, the nuclear lamins which plays an
215 integral role in the maintenance of genome integrity and induction of apoptosis was also
216 disrupted in the presence of rotenone, a phenomenon that was reversed in the presence of
217 PJ34 (Fig. 3G).

218 To confirm DNA-damage induced PARP hyperactivation, we next sought to analyze the
219 level of poly (ADP-ribose) (PAR) formation in rotenone treated cells [41]. As indicated in Fig. 3H,
220 there was a significant elevation of PAR formation at 24 h post-rotenone treatment that was
221 dramatically prevented in the presence of PJ34. Next, we performed a time-dependent analysis
222 of PAR formation in rotenone treated cells to determine whether PARP hyperactivation
223 preceded apoptosis and correlated with the early drop in $NAD^+$ levels. A robust increase in
224 PARylation was observed as early as 4 h following rotenone treatment (Fig. 3I) that strongly
225 suggested that ROS emanating from damaged mitochondria could result in sustained DNA
226 damage and PARP hyperactivation thus reducing $NAD^+$ levels in rotenone treated cells that is
227 prevented in the presence of PJ34. To further understand the importance of the role of PARPs
228 in rotenone-induced cell death, we conducted a siRNA mediated knockdown of PARP1 in SH-
229 SY5Y cells (Fig. 3J) and analyzed cell death in the presence of rotenone (Fig. 3K). There was a
230 significant (P value 0.0024) reversal of cell death following knock down of siPARP in rotenone

231 treated cells (Fig. 3K) further pointing towards the importance of PARP1 inhibition to prevent
232 rapid $NAD^+$ loss in rotenone mediated cell death.
233
234 **Prior incubation of cells with PJ34 prevented the activation of the NADase Sarm1 following**
235 **rotenone treatment**
236 Previous reports suggested that the NADase Sarm1 is required for rotenone induced cell
237 death [9,10] but the mechanism remains poorly understood. Here we observed increased
238 Sarm1 expression at 24 h post-rotenone treatment in the HEK293 cells but there was no
239 induction of Sarm1 at the earlier time points in both HEK293 and SH-SY5Y cells (Fig. 4A and B)
240 indicating that mitochondrial dysfunction and deregulation of autophagy machinery occurred
241 prior to Sarm1 induction in these cells. We also observed increased Sarm1 expression in 3T3
242 cells (Fig. S3A) but the levels were several folds lower than HEK293 cells which may account for
243 greater resistance of these cells to rotenone induced cell death (Fig. S3B). Interestingly,
244 transfection of HEK293 cells with siSarm1 resulted in partial reversal of rotenone induced cell
245 death (Fig. S3C) that indicated that Sarm1 could be a primary mediator of rotenone induced cell
246 death in non-neuronal cells as well. Although one of the Sarm1 antibodies was previously
247 standardized in western blot assay in primary neurons, these antibodies yielded non-specific
248 bands in western blot assay of HEK293 cells. Thus, in order to confirm Sarm1 knockdown by
249 siRNA transfection, we performed a real time analysis of the Sarm1 gene which showed a
250 significant reduction in Sarm1 expression (Fig. S3D). We further evaluated Sarm1 protein levels
251 in SH-SY5Y cells using an antibody that worked well in immunofluorescence studies in these
252 cells and observed an increase in the Sarm1 protein levels at 24 h post rotenone treatment (Fig.

253 4C Lower Panel) compared to 4 h (Fig. 4C Upper Panel) further strengthening the observation
254 that Sarm1 induction is a late event following rotenone treatment.

255 It has been previously shown that exogeneous addition of the $NAD^+$ precursor
256 nicotinamide riboside (NR) reverses axonal degeneration induced by overexpressed Sarm1 [42].
257 To understand whether NR had a similar effect on rotenone induced cell death in HEK293 cells,
258 we pre-incubated the cells with 1 mM NR for 1 h followed by addition of rotenone for 24 h. Our
259 results indicated that pre-incubation with NR had little or no effect on rotenone induced cell
260 death (Fig. 4D). We hypothesized that NR is probably being rapidly used up and hence cannot
261 combat the early $NAD^+$ loss that is further exacerbated following Sarm1 activation. Hence, we
262 exogenously added NR at 6 h to the cells that were previously pre-incubated with NR followed
263 by rotenone treatment. We also supplemented NR at low doses (0.5 mM) at 3 h and 6 h to
264 avoid the accumulation of NMN (nicotinamide mononucleotide) due to excess NR
265 supplementation. However, supplementing NR at different time points and with different doses
266 had no significant effect on rotenone induced cell death in the HEK293 cells (Fig. 4D). These
267 results indicated the importance of early $NAD^+$ loss induced by PARP1 hyperactivation in
268 rotenone mediated cell death. This is consistent with the recent Cryo EM observations in vitro
269 that loss of $NAD^+$ may release the autoinhibition of the ARM domain of Sarm1 by $NAD^+$ leading
270 to triggering of its NADase activity [30]. In line with this observation, we next sought to analyze
271 whether reversal of cell death and restoration of cellular $NAD^+$ levels by PJ34 correlated with
272 Sarm1 induction. Real-time PCR analysis of PJ34 treated cells followed by rotenone treatment
273 resulted in a prominent decrease in expression of Sarm1 at 24 h post treatment (Fig. 4E). It has
274 been demonstrated recently that cleavage of $NAD^+$ by Sarm1 results in the production of cADPR

275 [43, 44]. To understand whether the increased Sarm1 levels correlated with its activation, we
276 measured the cADPR levels in the neuronal SH-SY5Y cells at 24 post rotenone treatment. We
277 found a significant increase in cADPR levels following rotenone treatment that was reduced but
278 not completely abrogated in the presence of PJ34 in these cells (Fig. 4F).

279 Since Sarm1 has been shown to stabilize on depolarized mitochondria [45], we
280 proceeded to check its localization at the mitochondria using co-staining with the Cox IV
281 antibody following rotenone treatment in the presence and absence of PJ34. We show here for
282 the first time that rotenone treatment induced translocation of Sarm1 to the mitochondria at
283 24 h post treatment as compared to DMSO treated controls (Fig. 4G) (Right Upper Panel) which
284 was confirmed by the Pearson's correlation coefficient (PCC) where there was a significant
285 increase in the mitochondrial co-localization of Sarm1 (Fig. 4G Right panel) in rotenone treated
286 cells. In continuation to our previous observation, we further observed a reduction in the Sarm1
287 protein levels alongwith reduced mitochondrial localization in these cells in the presence of
288 PJ34 (Fig. 4G). To check the status of Sarm1 protein levels in HEK293 cells, we transfected these
289 cells with FLAG-tagged full length Sarm1 followed by rotenone treatment. Interestingly,
290 rotenone treatment stabilized the Sarm1 protein in these cells at 24 h post treatment
291 compared to the untreated DMSO control cells as evident from the more intense staining of the
292 FLG-tagged Sarm1 (Fig. S3E).

293 To understand the importance of the temporal induction of Sarm1 as observed in both
294 HEK293 and SH-SY5Y cells, we asked whether PJ34 could still be functional in preventing
295 rotenone-induced cell death in cells overexpressing Sarm1. Our data suggests that in contrast
296 to the un-transfected cells, PJ34 could not reverse rotenone induced cell death in Sarm1-

297 overexpressed cells which point towards the importance of the early events leading up to
298 Sarm1 activation that may act as the final trigger of cell death driving the cells towards a point
299 of no-return.
300
301 **PJ34 restored mitochondrial homeostasis and prevented accumulation of damaged**
302 **mitochondria in rotenone treated HEK293 and SH-SY5Y cells**
303 Since we hypothesized that early mitochondrial damage could subsequently leads to
304 PARP1 hyperactivation via ROS induced oxidative DNA damage leading to early $NAD^+$ loss and
305 Sarm1 induction, we checked the status of mitochondria in rotenone treated cells exposed to
306 PJ34. Pre-incubation of cells with PJ34 prevented early loss of mitochondrial membrane
307 potential (Fig. 5A) as early as 4 h post rotenone treatment. To further confirm the role of PJ34
308 in the maintenance of mitochondrial homeostasis, we co-stained rotenone treated HEK293 cells
309 pre-incubated with PJ34 with Mitotracker green and Lysotracker red. Two populations of cells
310 were observed at 4 h as indicated in Fig. 5B. Cells showed intact mitochondrial staining as
311 indicated by mitotracker green staining in rotenone treated cells in the presence of PJ34 (Fig.
312 5B upper panel). However, it was interesting to note increased co-localization of mitotracker
313 green and lysotracker red in these cells as indicated by arrows (Fig. 5B lower panel) that maybe
314 due to improved lysosomal turnover of damaged mitochondria. This was also confirmed by the
315 Pearson's correlation coefficient (PCC) which showed higher mitochondrial co-localization with
316 the lysosomes (Fig. 5B, right panel) following PJ34 treatment in the presence of rotenone.
317 Restoration of mitochondrial puncta structure was also noted in PJ34 treated SH-SY5Y cells
318 followed by rotenone treatment (Fig. 5C). We further observed a decrease in the mitochondrial

319 ROS levels as early as 4 h post rotenone treatment in the presence of PJ34 (Fig. 5D) that was
320 accompanied by a significant decrease in the total cellular ROS levels in these cells (Fig. 5E) that
321 strengthened our hypothesis of increased ROS production via accumulation of damaged
322 mitochondria induced by rotenone.

323 Since PARP inhibition by PJ34 improved mitochondrial turnover within the lysosomes
324 which may subsequently lead to restoration of mitochondrial homeostasis [46], we sought to
325 analyze the status of autophagy following PARP inhibition. Both Western blot and confocal
326 microscopy analysis revealed a decrease in LC3B-II/I ratio (Fig. 5F) and reduced signal strength
327 of LC3B (indicated by white arrows) in the nucleus (Fig. 5G) 4 h following rotenone treatment in
328 the presence of PJ34. Since mitochondrial damage and turnover seems to be intricately linked,
329 we sought to further understand whether functional autophagic machinery is required for PJ34
330 mediated protection from rotenone induced cell death. To test this hypothesis, cells were pre-
331 incubated with chloroquine (an inhibitor of lysosomal acidification) and no reversal of cell death
332 induced by rotenone was observed in the presence of a combination of chloroquine and PJ34 in
333 HEK293 (Fig. 5H). Interestingly, stimulation of autophagy by rapamycin also could not overcome
334 rotenone induced cell death (Fig. 5I). Collectively, these results suggest that a functional
335 autophagy is intricately linked with cell death in rotenone treated cells that can be alleviated by
336 PJ34 by restoring cellular $NAD^+$ levels and cannot be achieved by stimulating autophagy alone.

337

338 **PARP inhibition by Olaparib prevented rotenone induced neurotoxicity and reversed**
339 **rotenone induced locomotor deficits in 1-day old *Drosophila melanogaster***

340 In order to strengthen our understanding on the effect of PARP inhibition, apart from
341 PJ34 treatment and siPARP1 mediated knockdown assays, we further extended our studies with
342 another PARP inhibitor Olaparib. Although both PJ34 and Olaparib are known to inhibit PARP
343 catalytic activity [47,48], Olaparib has also been shown to induce PARP-DNA trapping [49] and
344 induce DNA damage in a dose-dependent manner. Hence, before we proceeded to understand
345 the effect of Olaparib in rotenone induced neurotoxicity, we first exposed SH-SY5Y cells to
346 increasing dose of Olaparib and measured the induction of cell death. Our results revealed that
347 a dose of 50 μM induced around 30% cell death in these cells. Hence, we chose a sub-optimal
348 dose of 20 μM to study the effect of olaparib on rotenone induced cell death (Fig. 6A). Pre-
349 incubation of cells with Olaparib followed by rotenone treatment significantly reversed
350 rotenone induced cell death in SH-SY5Y cells at 24h post treatment (Fig. 6B). To further
351 understand the physiological relevance of PARP inhibition by Olaparib in rotenone induced
352 pathological conditions, we extended our data in the fruitfly *Drosophila melanogaster*. Olaparib
353 has shown promise as an anti-cancer chemotherapeutic drug and is sold under the trade name
354 Lynparza to treat ovarian cancer 33[50,51]. Due to its known prospect in drug repurposing, we
355 selected Olaparib for PARP inhibition instead of PJ34 in our fly studies.

356 Our previous study has shown progressive locomotor deficits accompanied by dSarm
357 induction in $w^{1118}$ flies exposed to rotenone [9]. We first conducted a dose dependent analysis
358 of Olaparib due to the unavailability of such data in flies and measured its effect on fly survival
359 and selected the doses 50 and 100 μM for further analysis with rotenone. Our results indicated
360 that 1-day old flies exposed to 100 μM Olaparib in the presence of 200 μM of rotenone (Fig. 6C)
361 exhibited significant reversal in their climbing ability at 5, 10 and 20-days post exposure (Fig.

362 6D-F). We further observed heightened survival of flies in the presence of 100 μM Olaparib in
363 the presence of rotenone at 10 and 20-days post exposure (Fig. G and H). To check the status of
364 dSarm in these flies, we conducted a real time PCR analysis of the fly heads at 5 days post
365 rotenone treatment in the presence or absence of Olaparib. Our results show that Olaparib
366 prevented rotenone-mediated dSarm induction in younger flies. This is the first observation of
367 the effect of PARP inhibition by Olaparib in the reversal of rotenone induced locomotor deficits
368 in flies and further highlights the importance of PARP inhibitors in modulating rotenone
369 induced pathological conditions.
370
371 **Discussion**
372 $NAD^+$ is a critical factor in the regulation of cellular homeostasis including DNA repair,
373 mitochondrial function and autophagy [46, 52] but no single study has linked these processes
374 together. Rotenone, a potent inhibitor of mitochondrial complex I activity, induces loss of
375 mitochondrial membrane potential and stimulates the production of reactive oxygen species
376 (ROS) but the time-dependent regulation of these processes has not been discussed. A few
377 earlier studies have shown that addition of $NAD^+$ reduces rotenone induced cell death [53]
378 which is an important observation but how $NAD^+$ regulate life/death decision following
379 rotenone treatment is not known. These are important preliminary evidences linking cellular
380 $NAD^+$ levels with mitochondrial dysfunction ultimately leading to cell death especially in the
381 context of mitochondrial complex I inhibition by rotenone. Recent studies on the NADase
382 Sarm1 have implied that $NAD^+$ breakdown by Sarm1 could be a key event in rotenone induced
383 cell death. However, although the isoquinoline inhibitor of Sarm1 (DSRM-3716) could

384 significantly reverse rotenone induced axonal degeneration, defects within the mitochondria
385 persisted indicating that there could be other regulators of mitochondrial function in these cells
386 which act in a concerted manner to stimulate cell death [10]. Taking cues from these
387 observations, here we have attempted to dissect the temporal regulation of mitochondrial
388 dysfunction, ROS production and Sarm1 induction and how $NAD^+$ orchestrates these processes
389 in rotenone induced cell death.

390 Mitochondrial health and homeostasis are vital towards cell survival and dysregulation
391 of mitochondrial function has been linked to several diseases ranging from neurodegenerative
392 disease to cancer [54] . Mitochondria are an important source of cellular ROS which mediates
393 redox signaling at physiological levels [7]. However, accumulation of ROS leads to mitochondrial
394 damage [20] which maybe perpetuated within the cells if these damaged organelles are not
395 effectively cleared primarily via the process of autophagy (often termed as “mitophagy”). To
396 understand the cause and effect of rotenone induced mitochondrial damage, we conducted a
397 time-dependent analysis in HEK293 and SH-SY5Y cells and observed an early defect in
398 mitochondrial homeostasis and heightened ROS production that could not be ameliorated by
399 the ROS scavenger NAC. This clearly implied that accumulating mitochondrial damage overrode
400 the scavenging capacity of NAC in these cells and the disintegrated but the intense staining
401 pattern of the mitochondria further strengthened this observation in both HEK293 and SH-SY5Y
402 cells. A further analysis clearly indicated that there exists a defect in autophagic flux following
403 rotenone treatment that may lead to an ineffective clearance of damaged mitochondria. Apart
404 from the early defect in autophagic flux, we observed an increased accumulation of
405 endogenous LC3B within the nucleus of rotenone treated cells. Such localization was not

406 observed in the overexpressed LC3 (mCherry-GFP-LC3) which formed puncta typical of
407 autophagic vacuoles within the cytoplasm following rotenone treatment. Such enhanced
408 nuclear localization of endogenous LC3 is previously unreported and is an interesting outcome
409 of rotenone induced autophagic defect that needs to be explored further.

410 It has been recently highlighted that the oxidation state of the important cellular co-
411 factor nicotinamide dinucleotide (NAD) undergoes alteration following metabolic stress [15] but
412 how $NAD^+$ levels may directly contribute to the driving of the autophagic flux or clearance of
413 damaged mitochondria is not clearly defined. The only direct evidence linking $NAD^+$ levels to
414 mitochondrial homeostasis has been studied in the context of Werner's syndrome where the
415 authors demonstrate that augmentation of $NAD^+$ leads to improved lifespan via the restoration
416 of mitophagy [55]. Although we hypothesized that the $NAD^+$ levels could drop following the
417 activation of Sarm1 NADase activity, the timing of heightened Sarm1 expression and these early
418 cellular defects could be not explained. Hence, we conducted a time dependent analysis of
419 mitochondrial function and $NAD^+$ status following rotenone treatment. Contrary to our
420 expectations, we observed a loss of $NAD^+$ levels as early as 2 h post rotenone treatment which
421 did not match with the time of Sarm1 induction and this early loss of $NAD^+$ could not be
422 reversed by replenishing the $NAD^+$ pool with prior incubation with nicotinamide riboside (NR), a
423 precursor of NAD. NR has a short half-life and it could be rapidly used up in the cells. However,
424 intermittent replenishment with NR only slightly reversed rotenone induced cell death strongly
425 indicating that other factors contributed to the rapid $NAD^+$ loss within these cells.

426 In order to understand what causes the early $NAD^+$ loss in rotenone treated cells, we
427 looked into other $NAD^+$-consuming enzymes within the cell. Besides the NADase Sarm1 and

428 CD38, the protein deacylase family of Sirtuins and PARPs are known $NAD^+$ consuming enzymes.
429 Hyperactivation of PARP1 has been shown to impede autophagy due to consumption of $NAD^+$
430 and blocking Sirt1 function, a key regulator of autophagy [56]. Our results demonstrated PARP
431 hyperactivation as early as 4 h post rotenone treatment that may account for rapid loss of $NAD^+$
432 in rotenone treated cells. To delineate the function of this PARP hyperactivation, we asked
433 whether PARP inhibitors could restore cellular $NAD^+$ levels and prevent rotenone-induced cell
434 death. Our results showed that prior incubation with the PARP inhibitor PJ34 but not the Sirt1
435 inhibitor EX527 significantly reversed rotenone induced cell death. Further, PJ34 not only
436 prevented depletion of cellular $NAD^+$ levels following rotenone treatment but also restored
437 mitochondrial homeostasis and reduced ROS production. Importantly, abrogating this early
438 accumulating energy depleted state prevented Sarm1 mRNA induction and a significant
439 reduction in Sarm1 protein levels was observed in rotenone treated cells in the presence of
440 PJ34. Sarm1 is known to possess an N-terminal mitochondrial localization signal and rotenone
441 induced the translocation of Sarm1 to the mitochondria which is known to occur under stressed
442 conditions that was significantly reversed in the presence of PJ34. Quite interestingly, recent
443 Cryo EM studies on Sarm1 structure and function has shown the presence of an auto-inhibitory
444 ARM domain that remains bound to $NAD^+$ and prevents the activation of the NADase containing
445 TIR domain of SARM1 [57]. The importance of PARP1 in rotenone induced cell death was also
446 confirmed in siRNA studies in SH-SY5Y cells where there was significant reversal in cell death at
447 24 h. Thus, it is strongly possible that this early loss of $NAD^+$ induced by PARP1 hyperactivation
448 following rotenone treatment may overcome this auto-inhibition subsequently leading to the
449 activation of Sarm1 and severe energy deficits within the cell.

450 We extended our studies to another PARP inhibitor, Olaparib which showed a similar
451 reversal in cell death in SH-SH5Y cells. The physiological relevance of our observation in the
452 cellular studies was strengthened by the fact that inhibiting PARP by Olaparib reversed
453 rotenone induced locomotor deficits in *Drosophila melanogaster* that was accompanied by
454 reduction in dSarm levels. Taken together, this is an important finding that correlates loss of
455 endogeneous $NAD^+$ levels with the expression/activation of intracellular Sarm1 in both
456 neuronal and non-neuronal cell lines as well in flies. This study also provides a very important
457 lead in the understanding the role of PARP inhibitors in modulating cellular energy homeostasis
458 and mitochondrial function as depicted in the proposed model (Fig. 7). It is possible that early
459 mitochondrial dysfunction induced by rotenone leads to ROS production and oxidative DNA
460 damage that leads to PARP activation. Sustained mitochondrial damage in the absence of
461 functional autophagy leads to ROS accumulation, PARP1 hyperactivation and further loss of
462 $NAD^+$. This loss of $NAD^+$ may remove the allosteric inhibition of the ARM domain of Sarm1 and
463 lead to activation of its TIR-NADase activity leading to further energy deficits and ultimately cell
464 death.

465 In conclusion, these observations could be an important step towards our
466 understanding of the metabolic regulation of mitochondrial function, the autophagy-apoptosis
467 network and Sarm1 activation by rapid loss of endogeneous $NAD^+$ levels induced by the
468 mitochondrial complex I inhibitor, rotenone.

469

470 **Materials and Methods**

471 **Cell lines, antibodies and chemicals -** HEK293 cells were obtained from the laboratory of Dr.
472 Abhik Saha (Presidency University Kolkata, India), SHSY-5Y cells were obtained from Dr. Oishee
473 Chakrabarti (Saha Institute of Nuclear Physics, Kolkata) and 3T3 cells obtained from Dr. Shubhra
474 Majumder (Presidency University, Kolkata). The cells were maintained in Dulbecco's modified
475 Eagle's medium (DMEM) (Gibco, Life Technologies) supplemented with 10% fetal bovine serum
476 (FBS) (Invitrogen) and 1% Penicillin-Streptomycin Solution (Sigma).

477 Mouse monoclonal antibodies against β-actin (ab8224), p62 (ab56416) and LC3 A/B
478 (ab128025), Cov IV (ab16056) and rabbit polyclonal antibody against anti-cleaved caspase-3
479 (ab2302) were obtained from Abcam. Rabbit polyclonal antibody for AIF (4642), PARP1 (46D11)
480 were obtained from Cell Signaling Technology Inc., rabbit polyclonal antibodies against Sarm1
481 was obtained from GeneTex for western blot analysis and Sarm1 (D2M5I) for staining was
482 obtained from Cell Signaling Technology Inc. Rabbit polyclonal antibodies against FLAG (F1804)
483 was purchased from Sigma and for PAR (MCA-1480) was purchased from Bio-Rad. The antibody
484 for the protein MANLAC2 (Lamin A/C) was developed by Morris, G.E. (DHSB Hybridoma product
485 MANLAC2 (10F8)) and obtained from the Developmental Studies Hybridoma Bank, created by
486 the NICHD and maintained at the University of lowa, Department of Biology, lowa City, IA
487 52242. In order to determine the DNA damage and apoptosis, the Apoptosis and DNA damage
488 (H2A.X(S139) + cleaved PARP1 + Anti-GAPDH) Western Blot Cocktail (ab131385) was obtained
489 from Abcam. Mouse and Rabbit polyclonal secondary antibodies were purchased from Abcam
490 (ab97023 and ab97051 respectively).

491 Mitochondrial complex I inhibitor rotenone (Sigma), pan caspase inhibitor Z-VAD (OMe)-
492 FMK (Abcam), PARP-1 inhibitor, PJ-34 hydrochloride (Abcam), SIRT1 inhibitor EX-527 (Abcam),

493 autophagy inhibitor Chloroquine diphosphate salt (Sigma), the autophagy stimulator Rapamycin
494 (Abcam) were used in this study at the indicated doses. Nicotinamide riboside (NR) was
495 procured from ChromaDex, USA.

496 **Cell viability Assay-** Cells were cultured in 24-well plates for 24 h and were treated with
497 rotenone at the indicated doses and time. In some experiments, cells were pre-incubated for 1
498 h with either PJ-34, EX-527, Chloroquine, Bafilomycin, Rapamycin, Z-VAD-FMK or NR prior to
499 the addition of rotenone. Wells in triplicate were incubated with the MTT reagent (Sigma) at
500 the specific time points at a concentration of 5 mg/ml. Following 2 h of incubation, the MTT
501 solution was aspirated and the cells were lysed in DMSO and the formation of formazan in each
502 well was determined in a plate reader (BioTek) at an absorbance of 540 nm. All results were
503 compared to DMSO treated controls or the solvent used for the assay.

504 **Plasmid and transfection assays –** Cells were seeded at a density of $0.4x10^5$ cells/well, 24 h
505 prior to transfection. Cells were transfected with pCMV6-Sarm1 with C-terminal Myc-DDK tag (a
506 kind gift from Dr. Karin Peterson, Rocky Mountain Laboratories, NIAID, NIH, USA) or Flag-N-TIR-
507 Sarm1 with Lipofectamine 2000 (Invitrogen), for 48 h using the manufacturer's protocol. To
508 measure the status of autophagy, HEK-293 cells were transfected with mCherry-GFP-LC3 (a kind
509 gift from Rupak Datta, IISER Kolkata) for 24 hours followed by treatment with rotenone for 24
510 h.

511 siRNAs for PARP1 (#6304) were purchased from Cell Signaling Technology Inc. HEK293
512 and SH-SY5Y cells were seeded at a density of 0.4*10^6 in a 24-well plate, 24 h prior to
513 transfection. HEK293 and SH-SY5Y cells were transfected with siRNA (100 nM) for 24 h followed
514 by treatment with rotenone for 24 h. Cell viability was assessed in these cells as described

515 previously and results compared with control siRNA (#6568) treated cells. Similarly, HEK293 and
516 SH-SY5Y cells were transfected with 25 nM siSARM (s23032, Ambion, life technologies) for 48 h
517 followed by 24 h rotenone treatment. All the siRNA silencing and plasmid transfection studies
518 was done with lipofectamine 2000 purchased from Thermo Fisher Scientific.

519 **Whole cell extracts and Immunoblot Analysis –** Cells were cultured in 6-well plates at a cell
520 density of 0.8 x $10^6$ per well 24 h prior to treatment as indicated. Following treatment, cells
521 were lysed in lysis buffer (150mM NaCl, 1% NP-40, 50mM Tris pH 8.0) containing a protease
522 inhibitor cocktail (Pierce, Thermo Fisher Scientific) for the preparation of whole cell extracts.
523 Protein concentration was estimated using the Bradford assay kit (Bio-Rad) and 15 μg of
524 protein/well were resolved on 12% SDS-PAGE and subsequently analyzed by immunoblot
525 analysis. Bands were detected by a chemiluminescent ECL system (Bio-Rad) and quantified by
526 Image J software.

527 **Immunofluorescence assay –** 12 mm cover slips were placed in 24-well plates and coated with
528 geltrex for 1 h before seeding. Cells were seeded at a density of 0.03 x $10^6$ cells/well 24 h prior
529 to the treatment. Following treatment, cells were washed with 1x PBS and fixed with solution
530 containing 4% paraformaldehyde and 0.2% Triton-X-100 for 10 min followed by blocking with
531 5% NDS buffer (normal donkey serum, 0.05% Triton-X-100 and 0.2 M Glycine) at room
532 temperature for 30 min. The cells were incubated with primary antibody at 4°C overnight
533 followed by incubation with secondary antibody (Alexa flour 488 or Alexa flour 594) for 1 h at
534 room temperature. Nucleus was stained with DAPI (Bio-Rad) for 5 min along with secondary
535 antibody and mounted with Fluoroshield Mounting Medium (Abcam) and sealed for analysis. In
536 case of live staining the cells were seeded in grooved 35 mm plates (Thermo Fisher Scientific) at

537 a density of 0.04 x $10^6$. After treatment, cells were incubated with Lysotracker red DND9 (Life
538 technologies), Mitotracker green FM (Life technologies), TMRM (Sigma) and Mitosox (Life
539 technologies) at 37°C for 15 min and then washed with 3x times in fresh DMEM followed by
540 incubation with Hoechst 33342 (Sigma) for 5 min and further analyzed by confocal imaging. All
541 images were acquired by DMi8 confocal laser scanning microscope (Leica-microsystems) and
542 images were analyzed using image J software.

543 **$NAD^+$/NADH Assay-** The total NAD concentration, $NAD^+$/NADH ratio and the concentration of
544 total $NAD^+$ and NADH was determined by NAD/NADH fluorometric assay kit from Abcam
545 (ab176723) following manufacture's protocol. The concentration of each component was
546 calculated from the standard curve obtained by the standard solutions provided in kit. As per
547 manufacturer's instruction, respective concentrations were calculated by the equations
548 described in the protocol that is Total (NAD/NADH) = (B/V) x D where B = total NAD/NADH
549 amount in the sample well (µM), V=sample volume added in the sample wells, D= sample
550 dilution factor. The $NAD^+$ concentration was calculated with the same method from the same
551 standard curve. $NAD^+$/NADH assay results were obtained from three independent experiments
552 for each sample.

553 **cADPR Assay-** The concentration of cADPR was measured by Amplite Fluorometric cADPR-
554 Ribose Assay Kit (20305) from AAT Bioquest. Briefly, SH-SY5Y cells were seeded at a density of
555 0.4x$10^5$ cells/well and grown for 24 h prior to treatment. Cells were treated with 5 µM of
556 rotenone for either 16 h or 24 h following which whole cell lysate was extracted as described
557 previously. Total protein levels were estimated by Bradford reagent (Bio-Rad). Prior to the
558 setting up the test experiment, a standard curve was prepared by the reagents provided in the

559 kit. Standards, blank controls and samples were added to black well plates (50 µl) followed by
560 the addition of 50 µl of ADPRC working solution in each well. After 1 h incubation at room
561 temperature in the dark, $NAD^+$ levels were detected by the addition of 40 µl of Quest fluor
562 probe into each well followed by 40 µl of Assay solution II and incubation for 20 mins in dark
563 followed by the addition of 30 µl of enhancer solution into each well. The fluorescence intensity
564 was monitored at an excitation and emission of 420/480 nm. cADPR concentration for the test
565 samples was expressed as µg of cADPR/µg of protein. cADPR assay results were collected from
566 three independent experiment for each sample.

567 **Measurement of total cellular ROS –** Intracellular ROS was measured by H2DCF-DA (Sigma,
568 D6883) After treatment, cell lysate was prepared by NP-40 lysis buffer and H2DCFDA was added
569 at a concentration of 50 µM and incubated for 1 h and fluorescence intensities were measured
570 at Ex/Em: 492/527 nm.

571 **qReal-Time PCR –** RNA samples were collected by standard Trizol (Sigma) method and cDNA
572 was prepared by Bio-Rad iScript cDNA synthesis kit. The real-time data was analysed and
573 quantified by CFX manager software (Bio-Rad). All the results were obtained from at least three
574 independent experiments. The mRNA expression levels of every gene were quantified and
575 normalized with reference gene. In case of some genes relative expression was plotted by ΔCT
576 method to compare the basal level and level after treatment in every sample to show the
577 difference in expression. In another case the expressions of genes expressed as fold change
578 with respect to control samples by ΔΔCT method to determine the increase in the expression
579 with respect to control samples. The RT-PCR results were analysed by Bio-Rad CFX manager.
580 All the results were obtained from at least three independent experiments.

581 **Fly survival and negative geotaxis assay-**$W^{1118}$ flies were a generous gift from Dr. Rupak Dutta,
582 IISER, Kolkata. Both male and female flies were grown at 22° C and 12-h light/dark cycle in
583 incubator in standard corn meal-agar diet and changed every 3-5 days. Rotenone and Olaparib
584 was freshly prepared as 100 mM stock solution in DMSO. Flies were transferred to rotenone or
585 Olaparib containing fresh medium every 2-3 days to monitor survival and locomotor deficit.

586 For the survival assay 1-day old flies were transferred to DMSO, rotenone and rotenone
587 -Olaparib containing fresh medium. The total number of flies alngwith the dead and viable ones
588 were counted at 3-day interval and the percentage of survival was calculated up to 20 days for
589 each set. Three different sets were prepared per experiment.

590 The negative geotaxis assay was performed in a similar manner to that published by
591 Gargano et al (Gargano et al., 2005) with minor modifications. At least 20 treated and 20
592 control flies were transferred once a day in the early afternoon without anesthesia into a
593 vertical glass climbing vial (length, 25cm; diameter, 3cm) to perform the assay. The climbing
594 vials were placed in a rectangular frame in order to keep them upright. After a ten-minute
595 acclimation period, the vials were tapped three times to initiate the negative geotaxis assay.
596 After 10 s, the percentage of flies crossing the 5 cm mark was noted for each trial. This
597 procedure was repeated a total of ten times. All behavioral experiments were performed at
598 room temperature under standard light conditions.

599 **RNA isolation and qRT-PCR from fly samples-** For analysis of dSarm expression, fly heads were
600 collected from 1-day old flies at 5-days post rotenone treatment in the presence or absence of
601 Olaparib and crushed in a mortar-pestle with TRIZOL. The cDNAs were prepared by iScript cDNA
602 synthesis kit from Bio-Rad and the mRNA expressions were measured by drosophila specific

603 primers by ΔΔCT method as discussed in above and analyzed by CFX manager (Bio-Rad). All
604 results were collected from at least three independent samples.
605 **Statistical Analysis**- All statistical analysis was performed using GraphPad Prism version 7.00 for
606 Windows (GraphPad Software, La Jolla, CA, USA). The results are presented as mean ± SEM
607 (standard error of mean) of at least three independent experiments performed in triplicate.
608 Statistical significance was measured by one-way analysis of variance (ANOVA) with Bonferroni
609 posttest. Asterisks indicate levels of significance (*$p < 0.05$, **$p < 0.01$ and ***$p < 0.001$).
610

611 **Acknowledgements**

612 The authors would like to thank Rupak Datta, Abhik Saha and Shubhra Majumder for their
613 insightful comments during the preparation of the manuscript and for providing several
614 reagents. The work was funded by extramural funding from Dept. of Biotechnology, India
615 (#BT/PR10983/BRB/10/1282/2014) to PM. AS is a recipient of UGC-NET fellowship [F.16-
616 6(Dec.2016)/2017(NET)] and SD is a recipient of CSIR-NET fellowship [08/155(0085)-2020-EMR-
617 I] from Govt. of India.
618

619 **Conflict of interest**: The authors declare no conflict of interest
620

621 **Author contribution**

622 PM conceived the work and AS, MS, SD and PD performed the experiments. AS and PM wrote
623 the manuscript and prepared the figures and PM revised the entire manuscript.
624

625 **References**

1 A. H. V. Schapira, J. M. Cooper, D. Dexter, J. B. Clark, P. Jenner, and C. D. Marsden, "Mitochondrial Complex I Deficiency in Parkinson's Disease," *J. Neurochem.*, vol. 54, no. 3, pp. 823–827, 1990, doi: 10.1111/j.1471-4159.1990.tb02325.x.

2 P. M. Keeney, J. Xie, R. A. Capaldi, and J. P. Bennett, "Parkinson's disease brain mitochondrial complex I has oxidatively damaged subunits and is functionally impaired and misassembled," *J. Neurosci.*, vol. 26, no. 19, pp. 5256–5264, 2006, doi: 10.1523/JNEUROSCI.0984-06.2006.

3 H. Ueno, H. Miyoshi, M. Inoue, Y. Niidome, and H. Iwamura, "Structural factors of rotenone required for inhibition of various NADH-ubiquinone oxidoreductases," *Biochim. Biophys. Acta - Bioenerg.*, vol. 1276, no. 3, pp. 195–202, 1996, doi: 10.1016/0005-2728(96)00078-3.

4 N. Li *et al.*, "Mitochondrial complex I inhibitor rotenone induces apoptosis through enhancing mitochondrial reactive oxygen species production," *J. Biol. Chem.*, vol. 278, no. 10, pp. 8516–8525, 2003, doi: 10.1074/jbc.M210432200.

5 S. Tada-Oikawa, Y. Hiraku, M. Kawanishi, and S. Kawanishi, "Mechanism for generation of hydrogen peroxide and change of mitochondrial membrane potential during rotenone-induced apoptosis," *Life Sci.*, vol. 73, no. 25, pp. 3277–3288, 2003, doi: 10.1016/j.lfs.2003.06.013.

6 Y. Tsujimoto and S. Shimizu, "Role of the mitochondrial membrane permeability transition in cell death," *Apoptosis*, vol. 12, no. 5, pp. 835–840, 2007, doi: 10.1007/s10495-006-0525-7.

7 D. B. Zorov, M. Juhaszova, and S. J. Sollott, "Mitochondrial reactive oxygen species (ROS)

648 and ROS-induced ROS release," *Physiol. Rev.*, vol. 94, no. 3, pp. 909–950, 2014, doi:
649 10.1152/physrev.00026.2013.
650 8 R. Pal, T. O. Monroe, M. Palmieri, M. Sardiello, and G. G. Rodney, "Rotenone induces
651 neurotoxicity through Rac1-dependent activation of NADPH oxidase in SHSY-5Y cells,"
652 *FEBS Lett.*, vol. 588, no. 3, pp. 472–481, 2014, doi: 10.1016/j.febslet.2013.12.011.
653 9 M. Sur *et al.*, "Sarm1 induction and accompanying in fl ammatory response mediates
654 age-dependent susceptibility to rotenone-induced neurotoxicity," *Cell Death Discov.*,
655 2018, doi: 10.1038/s41420-018-0119-5.
656 10 R. O. Hughes *et al.*, "Small Molecule SARM1 Inhibitors Recapitulate the SARM1−/−
657 Phenotype and Allow Recovery of a Metastable Pool of Axons Fated to Degenerate," *Cell*
658 *Rep.*, vol. 34, no. 1, p. 108588, 2021, doi: 10.1016/j.celrep.2020.108588.
659 11 J. Gerdts, E. J. Brace, Y. Sasaki, A. DiAntonio, and J. Milbrandt, "SARM1 activation triggers
660 axon degeneration locally via NAD+ destruction," *Science (80-. ).*, vol. 348, no. 6233, pp.
661 453–457, 2015, doi: 10.1126/science.1258366.
662 12 D. W. Summers, D. A. Gibson, A. DiAntonio, and J. Milbrandt, "SARM1-specific motifs in
663 the TIR domain enable NAD+ loss and regulate injury-induced SARM1 activation," *Proc.*
664 *Natl. Acad. Sci. U. S. A.*, vol. 113, no. 41, pp. E6271–E6280, 2016, doi:
665 10.1073/pnas.1601506113.
666 13 K. Essuman, D. W. Summers, Y. Sasaki, X. Mao, A. DiAntonio, and J. Milbrandt, "The
667 SARM1 Toll/Interleukin-1 Receptor Domain Possesses Intrinsic NAD+ Cleavage Activity
668 that Promotes Pathological Axonal Degeneration," *Neuron*, vol. 93, no. 6, pp. 1334-
669 1343.e5, 2017, doi: 10.1016/j.neuron.2017.02.022.

14 M. Mink, B. Fogelgren, K. Olszewski, P. Maroy, and K. Csiszar, “A Novel Human Gene ( SARM ) at Chromosome 17q11 Encodes a Protein with a SAM Motif and Structural Similarity to Armadillo / ᴺL -Catenin That Is Conserved in Mouse , Drosophila , and Caenorhabditis elegans,” vol. 244, pp. 234–244, 2001, doi: 10.1006/geno.2001.6548.

15 C. C. S. Chini, J. D. Zeidler, S. Kashyap, G. Warner, and E. N. Chini, “Evolving concepts in NAD+ metabolism,” *Cell Metab.*, vol. 33, no. 6, pp. 1076–1087, 2021, doi: 10.1016/j.cmet.2021.04.003.

16 E. S. Hwang and S. Y. Hwang, “Cellular nad+ level: A key determinant of mitochondrial quality and health,” *Ann. Geriatr. Med. Res.*, vol. 21, no. 4, pp. 149–157, 2017, doi: 10.4235/agmr.2017.21.4.149.

17 S. Amjad *et al.*, “Role of NAD+ in regulating cellular and metabolic signaling pathways,” *Mol. Metab.*, vol. 49, no. February, p. 101195, 2021, doi: 10.1016/j.molmet.2021.101195.

18 C. L. Hsieh *et al.*, “Nicotinamide Increases Intracellular NAD+ Content to Enhance Autophagy-Mediated Group A Streptococcal Clearance in Endothelial Cells,” *Front. Microbiol.*, vol. 11, no. February, pp. 1–13, 2020, doi: 10.3389/fmicb.2020.00117.

19 C. Cantó, K. J. Menzies, and J. Auwerx, “NAD+ Metabolism and the Control of Energy Homeostasis: A Balancing Act between Mitochondria and the Nucleus,” *Cell Metab.*, vol. 22, no. 1, pp. 31–53, 2015, doi: 10.1016/j.cmet.2015.05.023.

20 G. Ashrafi and T. L. Schwarz, “The pathways of mitophagy for quality control and clearance of mitochondria,” *Cell Death Differ.*, vol. 20, no. 1, pp. 31–42, 2013, doi: 10.1038/cdd.2012.81.

21 R. Zeng *et al.*, “Icariin-mediated activation of autophagy confers protective effect on

692 rotenone induced neurotoxicity in vivo and in vitro," *Toxicol. Reports*, vol. 6, no.
693 February, pp. 637–644, 2019, doi: 10.1016/j.toxrep.2019.06.014.
694 22 S. Hurtado-Bagès, G. Knobloch, A. G. Ladurner, and M. Buschbeck, "The taming of PARP1
695 and its impact on NAD+ metabolism," *Mol. Metab.*, vol. 38, no. February, p. 100950,
696 2020, doi: 10.1016/j.molmet.2020.01.014.
697 23 C. C. Szabo *et al.*, "Opportunities for the repurposing of PARP inhibitors for the therapy of
698 non-oncological diseases," 2018, doi: 10.1111/bph.13748.
699 24 A. M. Curry, D. S. White, D. Donu, and Y. Cen, "Human Sirtuin Regulators: The 'Success'
700 Stories," *Front. Physiol.*, vol. 12, no. October, pp. 1–16, 2021, doi:
701 10.3389/fphys.2021.752117.
702 25 M. Mashimo *et al.*, "The 89-kDa PARP1 cleavage fragment serves as a cytoplasmic PAR
703 carrier to induce AIF-mediated apoptosis," *J. Biol. Chem.*, vol. 296, p. 100046, 2021, doi:
704 10.1074/jbc.RA120.014479.
705 26 E. Komulainen *et al.*, "Parp1 hyperactivity couples DNA breaks to aberrant neuronal
706 calcium signalling and lethal seizures," *EMBO Rep.*, vol. 22, no. 5, pp. 1–12, 2021, doi:
707 10.15252/embr.202051851.
708 27 J. Zhang *et al.*, "Parkinson's disease is associated with oxidative damage to cytoplasmic
709 DNA and RNA in substantia nigra neurons," *Am. J. Pathol.*, vol. 154, no. 5, pp. 1423–1429,
710 1999, doi: 10.1016/S0002-9440(10)65396-5.
711 28 C. M. Chen *et al.*, "Increased oxidative damage in peripheral blood correlates with
712 severity of Parkinson's disease," *Neurobiol. Dis.*, vol. 33, no. 3, pp. 429–435, 2009, doi:
713 10.1016/j.nbd.2008.11.011.

714 29 M. Sporny, C. Mim, M. N. Isupov, and R. Zalk, “The Structural Basis for SARM1 Inhibition ,
715 and Activation Under Energetic Stress,” *eLife*, no. August, 2020, doi:
716 10.1101/2020.08.05.238287.
717 30 M. Bratkowski *et al.*, “Structural and Mechanistic Regulation of the Pro-degenerative
718 NAD Hydrolase SARM1,” *Cell Rep.*, vol. 32, no. 5, p. 107999, 2020, doi:
719 10.1016/j.celrep.2020.107999.
720 31 M. Sporny *et al.*, “Structural Evidence for an Octameric Ring Arrangement of SARM1,” *J.*
721 *Mol. Biol.*, vol. 431, no. 19, pp. 3591–3605, 2019, doi: 10.1016/j.jmb.2019.06.030.
722 32 E. Perales-Clemente *et al.*, “Five Entry Points of the Mitochondrially Encoded Subunits in
723 Mammalian Complex I Assembly,” *Mol. Cell. Biol.*, vol. 30, no. 12, pp. 3038–3047, 2010,
724 doi: 10.1128/mcb.00025-10.
725 33 M. Ott, J. D. Robertson, V. Gogvadze, B. Zhivotovsky, and S. Orrenius, “Cytochrome c
726 release from mitochondria proceeds by a two-step process,” *Proc. Natl. Acad. Sci. U. S.*
727 *A.*, vol. 99, no. 3, pp. 1259–1263, 2002, doi: 10.1073/pnas.241655498.
728 34 S. Pankiv *et al.*, “p62/SQSTM1 binds directly to Atg8/LC3 to facilitate degradation of
729 ubiquitinated protein aggregates by autophagy*[S],” *J. Biol. Chem.*, vol. 282, no. 33, pp.
730 24131–24145, 2007, doi: 10.1074/jbc.M702824200.
731 35 G. Runwal, E. Stamatakou, F. H. Siddiqi, C. Puri, Y. Zhu, and D. C. Rubinsztein, “LC3-
732 positive structures are prominent in autophagy-deficient cells,” *Sci. Rep.*, vol. 9, no. 1, pp.
733 1–14, 2019, doi: 10.1038/s41598-019-46657-z.
734 36 L. Lei *et al.*, “Inhibition or stimulation of autophagy affects early formation of lipofuscin-
735 like autofluorescence in the retinal pigment epithelium cell,” *Int. J. Mol. Sci.*, vol. 18, no.

736 4, pp. 1–18, 2017, doi: 10.3390/ijms18040728.

737 37 L. Sedlackova and V. I. Korolchuk, “The crosstalk of NAD, ROS and autophagy in cellular
738 health and ageing,” *Biogerontology*, vol. 21, no. 3, pp. 381–397, 2020, doi:
739 10.1007/s10522-020-09864-0.

740 38 M. Cea *et al.*, “Targeting NAD+ salvage pathway induces autophagy in multiple myeloma
741 cells via mTORC1 and extracellular signal-regulated kinase (ERK1/2) inhibition,” *Blood*,
742 vol. 120, no. 17, pp. 3519–3529, 2012, doi: 10.1182/blood-2012-03-416776.

743 39 D. Sharma *et al.*, “PARP1 exhibits enhanced association and catalytic efficiency with
744 γH2A.X-nucleosome,” *Nat. Commun.*, vol. 10, no. 1, 2019, doi: 10.1038/s41467-019-
745 13641-0.

746 40 L. J. Kuo and L. X. Yang, “γ-H2AX- A novel biomaker for DNA double-strand breaks,” *In*
747 *Vivo*, vol. 22, no. 3. pp. 305–310, 2008.

748 41 X. Luo and W. Lee Kraus, “On par with PARP: Cellular stress signaling through poly(ADP-
749 ribose) and PARP-1,” *Genes Dev.*, vol. 26, no. 5, pp. 417–432, 2012, doi:
750 10.1101/gad.183509.111.

751 42 Y. Sasaki, T. Nakagawa, X. Mao, A. DiAntonio, and J. Milbrandt, “NMNAT1 inhibits axon
752 degeneration via blockade of SARM1-mediated NAD+depletion,” *Elife*, vol. 5, no.
753 OCTOBER2016, pp. 1–15, 2016, doi: 10.7554/eLife.19749.

754 43 K. W. Ko, J. Milbrandt, and A. DiAntonio, “SARM1 acts downstream of
755 neuroinflammatory and necroptotic signaling to induce axon degeneration,” *J. Cell Biol.*,
756 vol. 219, no. 8 August, 2020, doi: 10.1083/JCB.201912047.

757 44 Y. Sasaki *et al.*, “cADPR is a gene dosage-sensitive biomarker of SARM1 activity in

758 healthy, compromised, and degenerating axons," *Exp. Neurol.*, vol. 329, no. January,
759 2020, doi: 10.1016/j.expneurol.2020.113252.
760 45 H. Murata, M. Sakaguchi, K. Kataoka, and N. Huh, "SARM1 and TRAF6 bind to and
761 stabilize PINK1 on depolarized mitochondria," 2013, doi: 10.1091/mbc.E13-01-0016.
762 46 J. A. Muñoz-Gámez *et al.*, "PARP-1 is involved in autophagy induced by DNA damage,"
763 *Autophagy*, vol. 5, no. 1, pp. 61–74, 2009, doi: 10.4161/auto.5.1.7272.
764 47 S. Zha, Z. Li, Q. Cao, F. Wang, and F. Liu, "PARP1 inhibitor (PJ34) improves the function of
765 aging-induced endothelial progenitor cells by preserving intracellular NAD+ levels and
766 increasing SIRT1 activity," *Stem Cell Res. Ther.*, vol. 9, no. 1, pp. 1–10, 2018, doi:
767 10.1186/s13287-018-0961-7.
768 48 E. Hocsak *et al.*, "PARP inhibition protects mitochondria and reduces ROS production via
769 PARP-1-ATF4-MKP-1-MAPK retrograde pathway," *Free Radic. Biol. Med.*, vol. 108, no.
770 April, pp. 770–784, 2017, doi: 10.1016/j.freeradbiomed.2017.04.018.
771 49 A. Sinha, S. Katyal, and T. M. Kauppinen, "PARP-DNA trapping ability of PARP inhibitors
772 jeopardizes astrocyte viability: Implications for CNS disease therapeutics,"
773 *Neuropharmacology*, vol. 187, no. January, p. 108502, 2021, doi:
774 10.1016/j.neuropharm.2021.108502.
775 50 L. Montemorano, D. S. Michelle, and L. K. Bixel, "Role of olaparib as maintenance
776 treatment for ovarian cancer: The evidence to date," *Onco. Targets. Ther.*, vol. 12, pp.
777 11497–11506, 2019, doi: 10.2147/OTT.S195552.
778 51 Z. Gu *et al.*, "ClC-3/SGK1 regulatory axis enhances the olaparib-induced antitumor effect
779 in human stomach adenocarcinoma," *Cell Death Dis.*, vol. 11, no. 10, 2020, doi:

780 10.1038/s41419-020-03107-3.

781 52 H. Massudi, R. Grant, G. J. Guillemin, and N. Braidy, " NAD + metabolism and oxidative
782 stress: the golden nucleotide on a crown of thorns ," *Redox Rep.*, vol. 17, no. 1, pp. 28–
783 46, 2012, doi: 10.1179/1351000212y.0000000001.

784 53 Y. Hong, H. Nie, and X. Wei, "NAD + Treatment Can Prevent Rotenone-Induced Increases
785 in DNA Damage , Bax Levels and Nuclear Translocation of Apoptosis-Inducing Factor in
786 Differentiated PC12 Cells," 2015, doi: 10.1007/s11064-015-1534-0.

787 54 F. Distelmaier *et al.*, "Mitochondrial complex i deficiency: From organelle dysfunction to
788 clinical disease," *Brain*, vol. 132, no. 4, pp. 833–842, 2009, doi: 10.1093/brain/awp058.

789 55 E. F. Fang *et al.*, "NAD+ augmentation restores mitophagy and limits accelerated aging in
790 Werner syndrome," *Nat. Commun.*, vol. 10, no. 1, 2019, doi: 10.1038/s41467-019-13172-
791 8.

792 56 K. H. Jang, Y. Hwang, and E. Kim, "Parp1 impedes sirt1-mediated autophagy during
793 degeneration of the retinal pigment epithelium under oxidative stress," *Mol. Cells*, vol.
794 43, no. 7, pp. 632–644, 2020, doi: 10.14348/molcells.2020.0078.

795 57 Y. Jiang, T. Liu, C. H. Lee, Q. Chang, J. Yang, and Z. Zhang, "The NAD+-mediated self-
796 inhibition mechanism of pro-neurodegenerative SARM1," *Nature*, vol. 588, no. 7839, pp.
797 658–663, 2020, doi: 10.1038/s41586-020-2862-z.

798

799 **Figure Legends**

800 **Fig. 1. Rotenone induced cell death in both non-neuronal and neuronal cells that was**
801 **independent of caspase-3 activation. (A and B)** MTT assay of cells treated with indicated doses of
802 rotenone in HEK293 (A) and SH-SY5Y (B) cells at 6h and 24h post treatment **(C)** SH-SY5Y cells treated
803 with 5 µM of rotenone for 24 h and stained with anti-tubulin antibody to visualize the neurite processes

following rotenone treatment. The results were compared with DMSO control samples. Scale bar represents 10 μm **(D)** Representative confocal images of HEK293 cells stained with anti-active Caspase-3 antibody (red) and DAPI (blue) in the presence of rotenone or DMSO control. Scale bar represent 25 μm. The right panel represents the percentage of active-caspase-3 positive cells in the presence of DMSO or 500 nM rotenone and results are representative of at least five individual fields per treatment **(E and F)** HEK293 (E) and SH-SY5Y cells (F) were pre-incubated with the pan-caspase inhibitor Z-VAD-(OMe)-FMK (20 μM) for 1 h prior to rotenone (500 nM or 5 μM respectively) treatment and cell viability was measured by MTT assay. All results are representative of atleast three independent experiments.

**Fig. 2. Rotenone induced cell death was accompanied by mitochondrial dysfunction, increased ROS accumulation and defective autophagy. (A)** (Left panel) Immunofluorescence analysis of HEK293 cells incubated with 100 nM TMRM to assess the mitochondrial membrane depolarization in DMSO control and rotenone treated cells at 4 h post-treatment. Scale bar represents 25 μm. (Right panel) Corrected total cell fluorescence (CTCF) values of TMRM intensity of control vs rotenone treated cells **(B)** Immunofluorescence analysis of SH-SY5Y cells stained with 100 nM of TMRM at 4 h post rotenone treatment and compared with DMSO control. Scale bar represents 10 μm. (Right panel) CTCF values of TMRM intensity of control vs rotenone treated cells **(C and D)** Immunofluorescence analysis of SH-SY5Y (C) and HEK293 (D) cells stained with 100 nM of Mitotracker Green at 4 h post rotenone treatment and compared with DMSO controls. Scale bar represents 10 μm (C) and 5 μm (D). Arrows indicate intact or disrupted mitochondrial punctas in the enlarged panel (C) or in D **(E)** Visualization of mitochondrial ROS production in HEK293 cells by staining with the mitochondria specific ROS indicator Mitosox red at 4 h post rotenone treatment. Scale bar represents 50 μm **(F)** Relative fluorescence intensity (RFI) as a measure of ROS production in HEK293 cells with and without pre-incubation with 1mM NAC followed by rotenone treatment. Total ROS level was measured by H2DCFDA assay and fluorescence intensities were measured at Ex/Em: 492/527 nm **(G and H)** MTT assay of HEK293 (G) and SH-SY5Y (H) cells in the presence or absence of NAC pre-treatment followed by rotenone treatment for 24 h **(I)** Immunofluorescence analysis of SH-SY5Y cells treated with rotenone for 24 h and stained with anti-AIF (red) antibody and DAPI (blue) to visualize the nuclear localization of AIF post rotenone treatment and compared to DMSO controls. Scale bar represents 25 μm. **(J)** Immunofluorescence assay of HEK293 cells stained with anti-LC3B (red), anti-p62 (green) antibodies and DAPI (blue) to compare the expression and localization of the autophagy proteins followed by rotenone treatment. Scale bar represents 25 μm in the left panel. The indicated cells are cropped to show the single cell localization of these proteins **(K)** Immunofluorescence assay of SH-SY5Y cells with anti-p62 (red), anti-Tubulin (green) antibodies and DAPI (blue) to assess p62 accumulation following rotenone treatment (5 μM) for 24 h **(L)** Immunofluorescence analysis of SH-SY5Y cells co-stained with mitotracker green and lysotracker red at 4 h post rotenone treatment to compare the colocalization of the mitochondria with the lysosome. Scale bar represents 10 μm (upper panel) and 6 μm (lower panel). **(M)** Autophagic flux determination in HEK293 cells with transient transfection with mCherry-EGFP-LC3B plasmid for 24 h followed by rotenone treatment for 4 h

**Fig. 3. Rotenone treatment resulted in depletion of cellular $NAD^+$ levels and PARP inhibition by PJ34 prevented rotenone-induced cell death in both HEK293 and SH-SY5Y cells. (A)** Determination of $NAD^+$/NADH ratios by fluorometric assay in HEK293 cells 24 h post rotenone (500 nM) treatment and compared with DMSO treated controls **(B)** Cell viability was measured using MTT assay in HEK293 cells pre-incubated for 1 h with 25 μM of the PARP inhibitor PJ34 followed by 500 nM of rotenone treatment for 24 h and the results were compared with DMSO control **(C)** Cell viability was measured using MTT assay in SH-SY5Y cells pre-incubated for 1 h with 50 or 100 μM of the PARP inhibitor PJ34 followed by 5

851 μM of rotenone treatment for 24 h and the results were compared with DMSO control **(D)** $NAD^+$/NADH
852 ratios by fluorometric assay in SH-SY5Y in an early time point to show the rapid loss of $NAD^+$ post
853 rotenone treatment and results were compared with samples pre-incubated with PJ34 (50 μM) to
854 determine the role of PARP inhibition **(E)** Cell viability assay in the presence of Sirt1 inhibitor EX-527
855 (25μM) in HEK293 cells. Cells were pre-incubated with EX-527 for 1 h followed by rotenone treatment
856 for 24 h **(F)** (Left panel) Immunoblot analysis of DNA damage and apoptosis marker proteins H2AX and
857 cleaved Parp1 respectively in rotenone treated cells with or without prior treatment with PJ-34. Gapdh
858 served as loading control. A cocktail antibody containing the proteins mentioned were used (Right
859 panel) Densitometric analysis to determine the relative protein levels with respect to the loading control
860 was performed in Image J software **(G)** Representative confocal images of SH-SY5Y cells pre-incubated
861 with PJ34 (50 μM) and immuno-stained with anti-Lamin(A/C) antibody (green) and DAPI (blue) to
862 visualize the nuclear lamin disintegration at 4 h post rotenone treatment and the results were compared
863 to DMSO and PJ34 only controls **(H)** (Left panel) Immunoblot analysis of PARP1 hyperactivation by
864 determining the PARylation levels. (Right panel) Densitometric analysis of PAR (Poly ADP Ribose chain)
865 to determine the relative level of PAR in indicative treatments **(I)** Immunoblot analysis of PARP1
866 hyperactivation in SH-SY5Y cells at the indicated time points. Densitometric analysis of PAR (right panel)
867 were performed in the samples to determine the relative level of PAR **(J)** (Left panel) Immunoblot
868 analysis of PARP1 to determine the level of knock-down by siRNA in SH-SY5Y cells (Right panel)
869 Densitometric analysis of siRNA knock-down samples for PARP1. β-Actin serve as loading control for
870 immunoblot analysis and the quantification performed by Image J software. **(K)** Cell viability assay in
871 PARP1 knock-down SH-SY5Y cells followed by rotenone treatment for 24 h and the results were
872 compared with control siRNA samples. Data are representative of at least three independent
873 experiments per panel.
874
875 **Fig. 4. Prior incubation of cells with PJ34 prevented the activation of the NADase Sarm1 following**
876 **rotenone treatment. (A and B)** Relative fold change of mRNA expression of Sarm1 gene at 4 and 24 h
877 post rotenone treatment in HEK293 (A) and at 4, 6, 16, 24 and 36 h post rotenone treatment in SH-SY5Y
878 cells (B). Gapdh was used as an internal control **(C)** Immunofluorescence analysis of endogenous Sarm1
879 (red) in the presence or absence of rotenone at 4 h (Upper panel) and 24 h (Lower panel) post-rotenone
880 treatment. Scale bar represents 25 μm for upper panel and 10 μm for lower panel. Nuclear staining is
881 represented with DAPI (blue) **(D)** HEK293 cells were pre-incubated with 1mM NR followed by rotenone
882 treatment for 24 h or intermittent replenishment with NR at the times indicated and MTT assay was
883 conducted to analyze percent cell death. Data are representative of at least three independent
884 experiments per panel **(E)** Relative fold change of mRNA expression of Sarm1 gene in rotenone treated
885 (24 h) HEK293 cells by qRT-PCR with respect to DMSO treated control samples in the presence or
886 absence of PJ34. Gapdh was used as an internal control **(F)** SH-SY5Y cells were treated with indicated
887 treatments for 24 h and cADPR levels were quantified by cADPR assay kit and the concentration of
888 cADPR was expressed as μM/μg of protein. Data are representative of at least three independent
889 experiments per panel **(G)** Representative confocal images (left panel) of SH-SY5Y cells treated with
890 rotenone in the absence or presence of PJ34 for 24 h and immunostained with anti-COXIV (green), anti-
891 Sarm (red) and DAPI (blue) to visualize the localization and levels of Sarm1 at the mitochondria after
892 indicated treatments. Comparative analysis of CTCF values was performed to quantify the intensities in
893 each sample. CTCF values were determined for at least fifteen fields for each sample (upper right panel).
894 The bottom right panel represents the colocalization of Sarm1 with COXIV. Pearsons' coefficients were
895 determined by Image J software for indicated treatments and compared with DMSO control **(H)** Cell
896 viability assay in FL-Sarm1 overexpressed SH-SY5Y cells transfected for 48 h followed by rotenone
897 treatment for 24 h in the presence or absence of PJ34 and the results were compared with control
898 untransfected samples. Data are representative of at least three independent experiments per panel.

899
900 **Fig. 5. PJ34 restored mitochondrial homeostasis and prevented accumulation of damaged**
901 **mitochondria in rotenone treated HEK293 and SH-SY5Y cells. (A)** Immunofluorescence analysis of
902 HEK293 cells incubated with 100 nM TMRM to assess the mitochondrial membrane depolarization in
903 control and rotenone treated cells in the presence or absence of PJ34 at 4 h post rotenone treatment.
904 Scale bar represents 25 μm **(B**) Immunofluorescence analysis of HEK293 cells co-stained with
905 mitotracker green and lysotracker red at 24 h post rotenone treatment to compare the colocalization of
906 the mitochondria with the lysosome in the presence or absence of PJ34. Scale bar represents 25 μm
907 (upper panel) and 6 μm (lower panel). The arrow represents the colocalization in rotenone and PJ34
908 treated cells and the degree of co-localization was quantified by determining Pearson's correlation
909 coefficient (PCC) by Image J software (right panel) **(C)** Representative confocal images of SH-SY5Y cells
910 incubated with mitotracker green (100 nM) to determine intactness of mitochondria with or without
911 PJ34 pre-treatment followed by rotenone. Scale bar represents 25 μm **(D)** Visualization of mitochondrial
912 ROS production in HEK293 cells by staining with the mitochondria specific ROS indicator Mitosox red at
913 4 h post rotenone treatment in the presence or absence of PJ34. Scale bar represents 50 μm **(E)**
914 Measurement of total ROS levels by H2DCFDA assay and at Ex/Em: 492/527 nm by DCFDA assay to
915 compare the overall ROS production in rotenone treated cells in the presence of absence of PJ34 **(F)**
916 Immunoblot analysis of the autophagy marker protein LC3B in HEK293 cells treated with rotenone (24 h)
917 in the presence or absence of PJ34. β-actin was used as a loading control **(G)** HEK293 cell co-stained with
918 anti-LC3B (red) and anti-p62 (green) and nuclear stain DAPI (blue) to visualize the localization of
919 autophagy marker proteins post rotenone treatment. Results were compared with DMSO control and
920 PJ-34 treated cells. Single-cell cropped images are shown. **(H)** Cell viability assay in the presence of
921 autophagic inhibitor chloroquine (50μM) with or without incubating the HEK293 cells with PJ34 prior to
922 rotenone treatment **(I**) Cell viability assay in HEK293 cells pre-incubated with the **a**utophagy inducer
923 Rapamycin (200 nM) prior to rotenone treatment for 24 h to determine the role of autophagy induction
924 in response to rotenone treatment. Data are representative of at least three independent experiments
925 per panel.
926
927 **Fig. 6. PARP inhibition by Olaparib prevented rotenone induced neurotoxicity and reversed rotenone**
928 **induced locomotor deficits in 1-day old *Drosophila melanogaster.* (A)** Dose dependent cell death
929 analysis of Olaparib in SH-SY5Y cells at 24 h post-treatment. The percentage of cell death was
930 determined by MTT assay to compare the cell death in indicated treatments **(B)** MTT assay of SH-SY5Y
931 cells treated with rotenone (5 μM) in the presence or absence of 20 μM of Olaparib (pre-treated for 1 h
932 prior to rotenone treatment) at 24 h post-treatment **(C)** Schematic representation of the experimental
933 setup in *Drosophila melanogaster* **(D-F)** Negative geotaxis assay of 1-day old flies at 5 (D), 10 (E) and 20
934 (F) days post exposure with DMSO, olaparib (100 μM), rotenone (200 μM) and rotenone + olaparib **(G-**
935 **H)** Survival assay of flies exposed as described in E-F. *** denotes significance between DMSO control
936 and rotenone exposed flies and *** denotes significance between rotenone and rotenone + olaparib
937 exposed flies**.** Results are representative of at least three independent set of experiments.
938
939 **Fig. 7. Proposed model of the study.** Addition of rotenone to the cells results in mitochondrial
940 depolarization and generation of reactive oxidative species (ROS). Excess ROS accumulation leads to
941 nuclear DNA damage and PARP1 activation that leads to depletion of $NAD^+$. This early loss of $NAD^+$
942 blocks autophagic flux resulting in accumulation of damaged mitochondria, thus perpetuating further
943 ROS production. In a vicious cycle this causes further DNA damage, PARP1 hyperactivation and
944 subsequent $NAD^+$ loss. This loss of $NAD^+$ is predicted to remove the allosteric inhibition on the pro-
945 apoptotic protein Sarm1 thus activating it. Sarm1 localizes to the depolarized mitochondria and induces

946 subsequent cell death. Prior incubation with the PARP inhibitor, PJ34 replenishes cellular $NAD^+$ levels,
947 restores mitochondrial homeostasis and prevents Sarm1 upregulation in the cells thus preventing
948 rotenone induced cell death. (*Created with BioRender.com*).
949

# Fig. 1

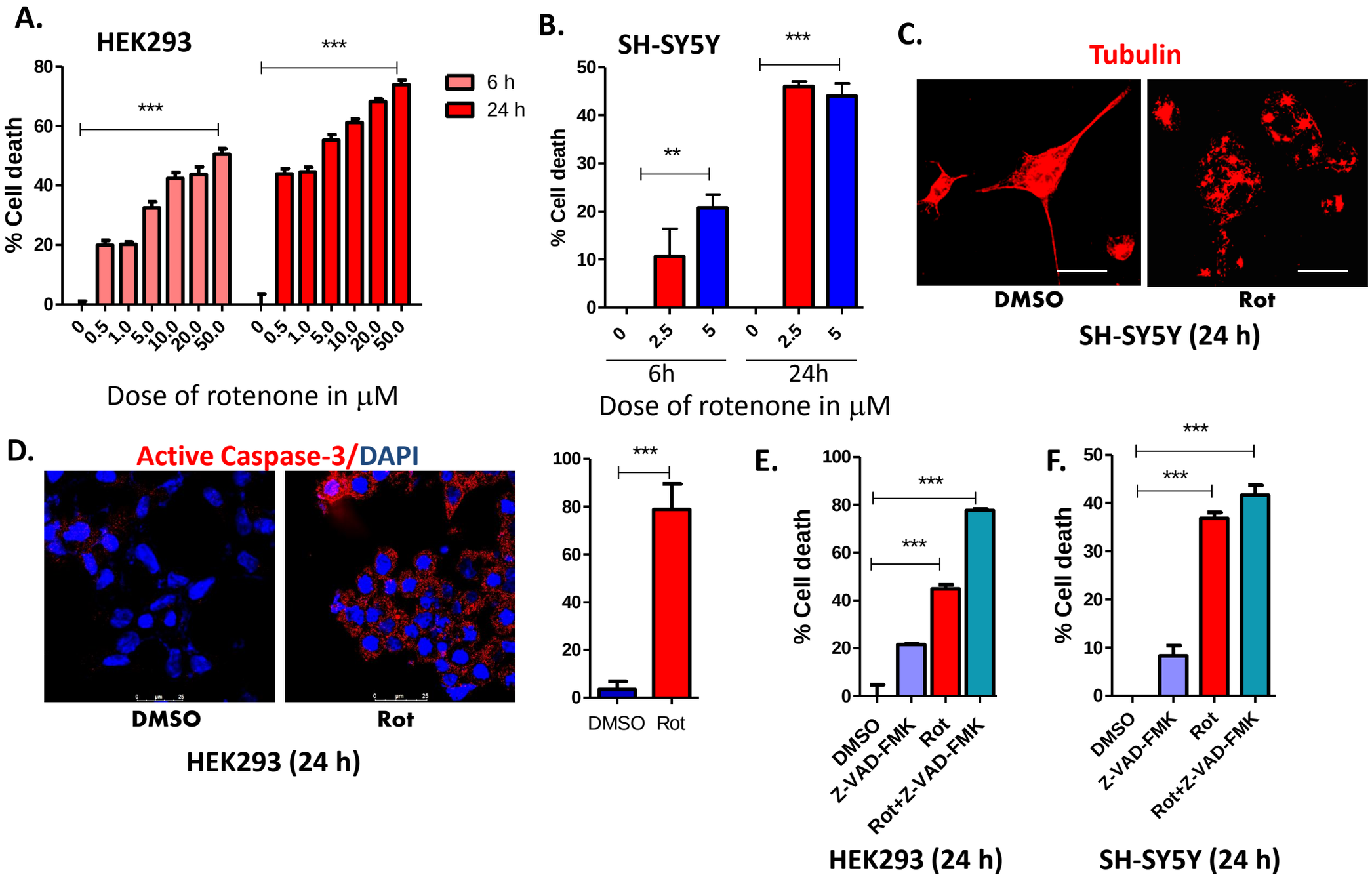
A.
HEK293
***
***
% Cell death
6 h
24 h
0
0.5
1.0
5.0
10.0
20.0
50.0
Dose of rotenone in μM
B.
SH-SY5Y
***
**
% Cell death
0
2.5
5
6h
24h
Dose of rotenone in μM
C.
Tubulin
DMSO
Rot
SH-SY5Y (24 h)
D.
Active Caspase-3/DAPI
DMSO
Rot
HEK293 (24 h)
***
DMSO
Rot
E.
***
***
% Cell death
DMSO
Z-VAD-FMK
Rot
Rot+Z-VAD-FMK
HEK293 (24 h)
F.
***
***
% Cell death
DMSO
Z-VAD-FMK
Rot
Rot+Z-VAD-FMK
SH-SY5Y (24 h)

Fig. 2

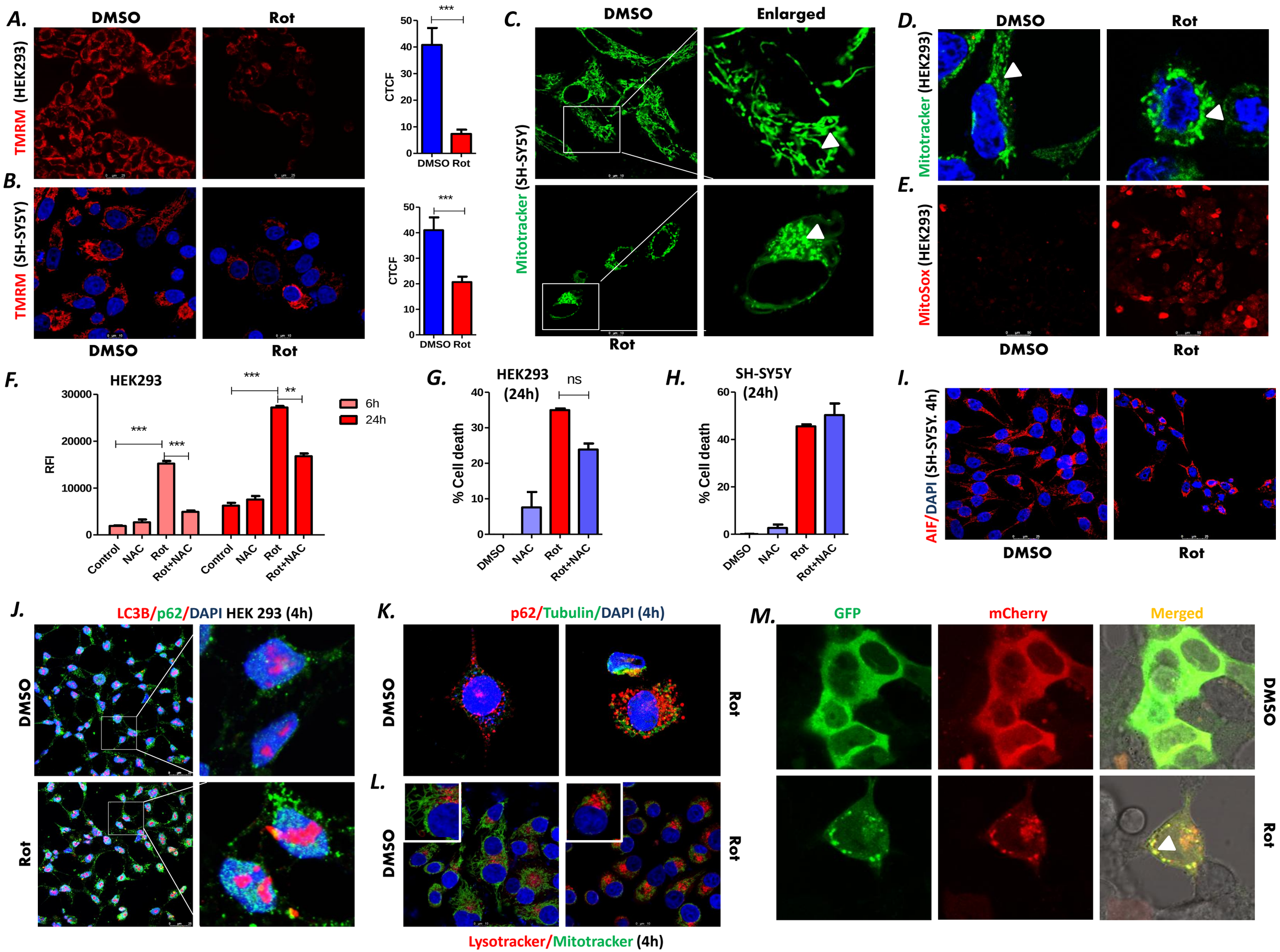
A.
DMSO
Rot
TMRM (HEK293)
CTCF
DMSO Rot
B.
TMRM (SH-SY5Y)
DMSO
Rot
C.
DMSO
Enlarged
Mitotracker (SH-SY5Y)
Rot
D.
DMSO
Rot
Mitotracker (HEK293)
E.
MitoSox (HEK293)
DMSO
Rot
F.
HEK293
RFI
6h
24h
Control
NAC
Rot
Rot+NAC
G.
HEK293 (24h)
ns
% Cell death
DMSO
NAC
Rot
Rot+NAC
H.
SH-SY5Y (24h)
% Cell death
DMSO
NAC
Rot
Rot+NAC
I.
AIF/DAPI (SH-SY5Y. 4h)
DMSO
Rot
J.
LC3B/p62/DAPI HEK 293 (4h)
DMSO
Rot
K.
p62/Tubulin/DAPI (4h)
DMSO
Rot
L.
DMSO
Rot
Lysotracker/Mitotracker (4h)
M.
GFP
mCherry
Merged
DMSO
Rot

Fig. 3

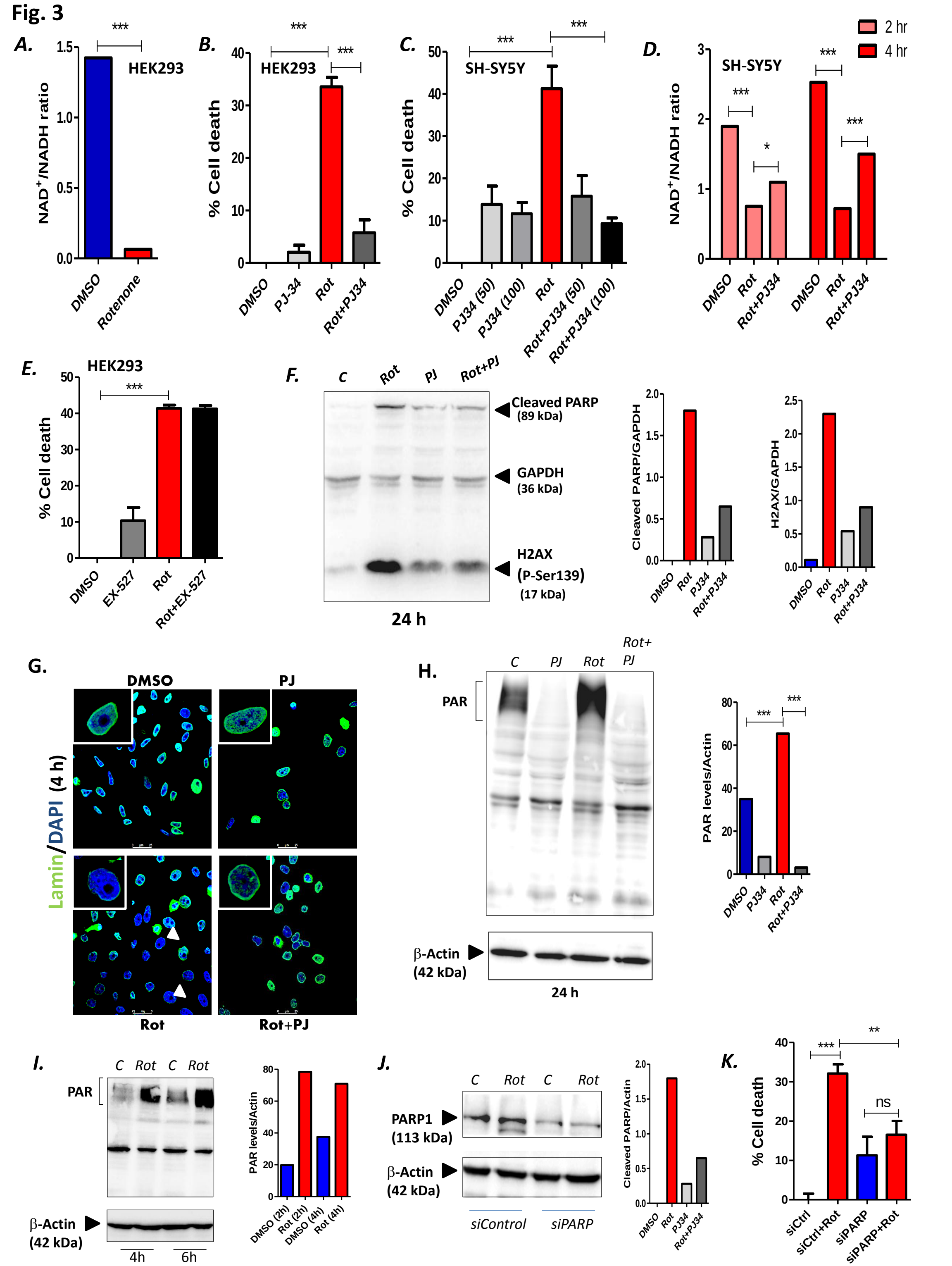
A.
HEK293
NAD+/NADH ratio
DMSO
Rotenone
B.
HEK293
% Cell death
DMSO
PJ-34
Rot
Rot+PJ34
C.
SH-SY5Y
% Cell death
DMSO
PJ34 (50)
PJ34 (100)
Rot
Rot+PJ34 (50)
Rot+PJ34 (100)
D.
SH-SY5Y
2 hr
4 hr
NAD+/NADH ratio
DMSO
Rot
Rot+PJ34
E.
HEK293
% Cell death
DMSO
EX-527
Rot
Rot+EX-527
F.
C
Rot
PJ
Rot+PJ
Cleaved PARP
(89 kDa)
GAPDH
(36 kDa)
H2AX
(P-Ser139)
(17 kDa)
24 h
Cleaved PARP/GAPDH
H2AX/GAPDH
DMSO
Rot
PJ34
Rot+PJ34
G.
DMSO
PJ
Lamin/DAPI (4 h)
Rot
Rot+PJ
H.
C
PJ
Rot
Rot+
PJ
PAR
β-Actin
(42 kDa)
24 h
PAR levels/Actin
DMSO
PJ34
Rot
Rot+PJ34
I.
C
Rot
C
Rot
PAR
β-Actin
(42 kDa)
4h
6h
PAR levels/Actin
DMSO (2h)
Rot (2h)
DMSO (4h)
Rot (4h)
J.
C
Rot
C
Rot
PARP1
(113 kDa)
β-Actin
(42 kDa)
siControl
siPARP
Cleaved PARP/Actin
DMSO
Rot
PJ34
Rot+PJ34
K.
% Cell death
ns
siCtrl
siCtrl+Rot
siPARP
siPARP+Rot

Fig. 4

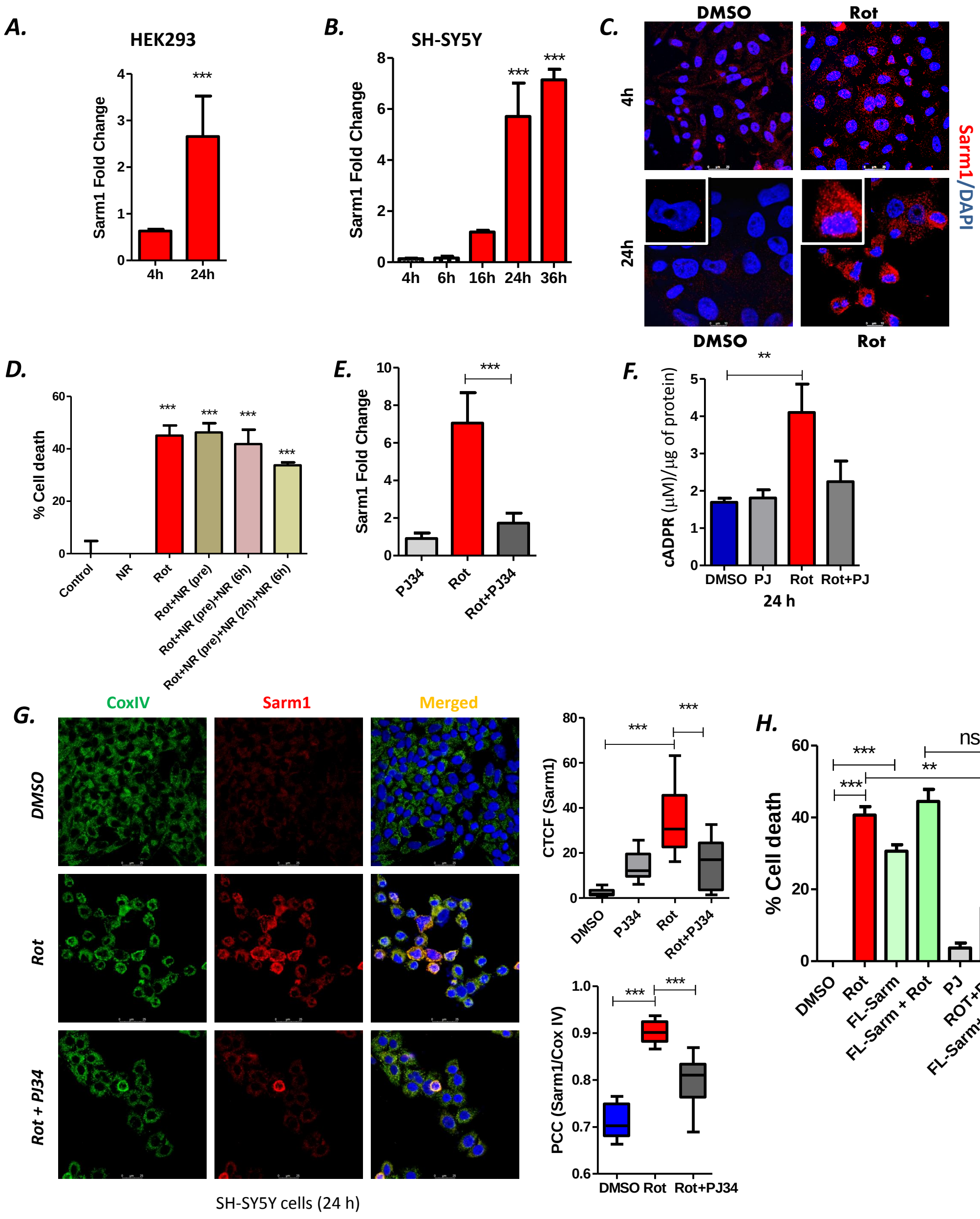
A.
HEK293
Sarm1 Fold Change
4h
24h
B.
SH-SY5Y
Sarm1 Fold Change
4h
6h
16h
24h
36h
C.
DMSO
Rot
4h
24h
Sarm1/DAPI
D.
% Cell death
Control
NR
Rot
Rot+NR (pre)
Rot+NR (pre)+NR (6h)
Rot+NR (pre)+NR (2h)+NR (6h)
E.
Sarm1 Fold Change
PJ34
Rot
Rot+PJ34
F.
cADPR (μM)/μg of protein)
DMSO
PJ
Rot
Rot+PJ
24 h
G.
CoxIV
Sarm1
Merged
DMSO
Rot
Rot + PJ34
SH-SY5Y cells (24 h)
CTCF (Sarm1)
DMSO
PJ34
Rot
Rot+PJ34
PCC (Sarm1/Cox IV)
DMSO
Rot
Rot+PJ34
H.
% Cell death
ns
DMSO
Rot
FL-Sarm
FL-Sarm + Rot
PJ
ROT+PJ
FL-Sarm+Rot+PJ

Fig. 5

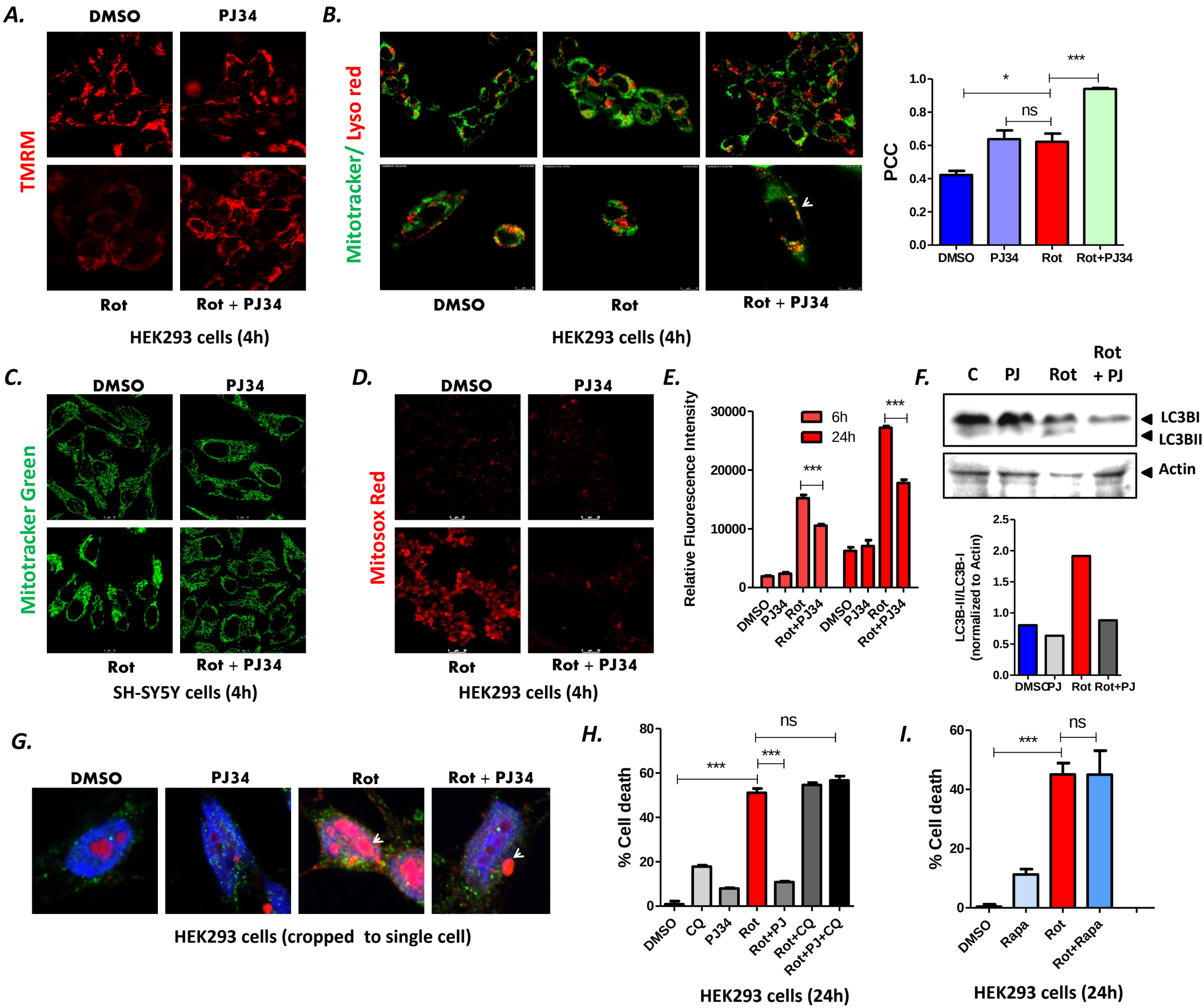
A.
DMSO
PJ34
TMRM
Rot
Rot + PJ34
HEK293 cells (4h)
B.
Mitotracker/ Lyso red
DMSO
Rot
Rot + PJ34
HEK293 cells (4h)
PCC
1.0
0.8
0.6
0.4
0.2
0.0
*
***
ns
DMSO
PJ34
Rot
Rot+PJ34
C.
DMSO
PJ34
Mitotracker Green
Rot
Rot + PJ34
SH-SY5Y cells (4h)
D.
DMSO
PJ34
Mitosox Red
Rot
Rot + PJ34
HEK293 cells (4h)
E.
Relative Fluorescence Intensity
30000
20000
10000
0
6h
24h
***
***
DMSO
PJ34
Rot
Rot+PJ34
DMSO
PJ34
Rot
Rot+PJ34
F.
C
PJ
Rot
Rot + PJ
LC3BI
LC3BII
Actin
LC3B-II/LC3B-I (normalized to Actin)
2.5
2.0
1.5
1.0
0.5
0.0
DMSO
PJ
Rot
Rot+PJ
G.
DMSO
PJ34
Rot
Rot + PJ34
HEK293 cells (cropped to single cell)
H.
% Cell death
80
60
40
20
0
***
***
ns
DMSO
CQ
PJ34
Rot
Rot+PJ
Rot+CQ
Rot+PJ+CQ
HEK293 cells (24h)
I.
% Cell death
60
40
20
0
***
ns
DMSO
Rapa
Rot
Rot+Rapa
HEK293 cells (24h)

Fig. 6

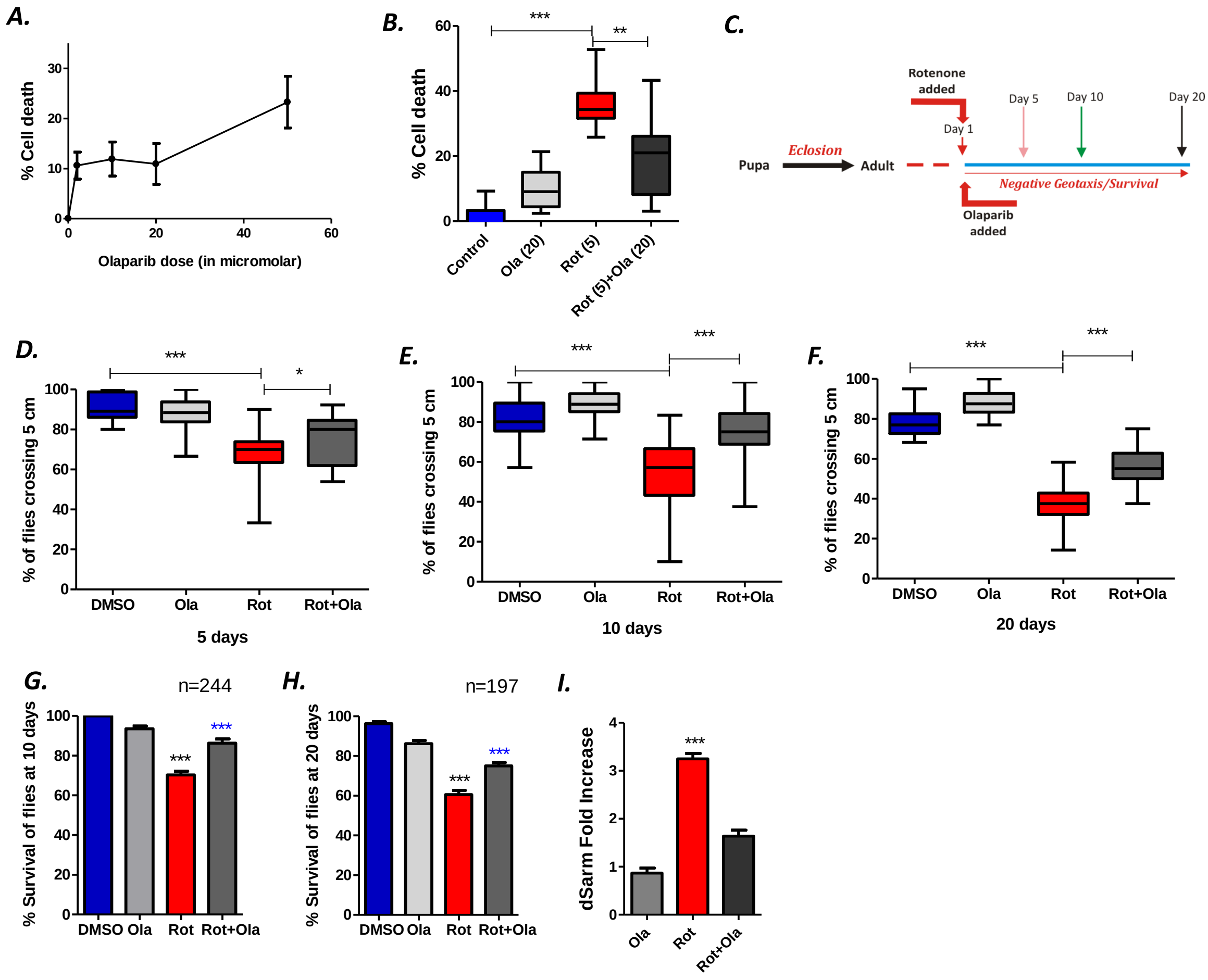
A.
% Cell death
Olaparib dose (in micromolar)
B.
% Cell death
Control
Ola (20)
Rot (5)
Rot (5)+Ola (20)
C.
Rotenone added
Day 1
Day 5
Day 10
Day 20
Pupa
Eclosion
Adult
Negative Geotaxis/Survival
Olaparib added
D.
% of flies crossing 5 cm
DMSO
Ola
Rot
Rot+Ola
5 days
E.
% of flies crossing 5 cm
10 days
F.
% of flies crossing 5 cm
20 days
G.
n=244
% Survival of flies at 10 days
H.
n=197
% Survival of flies at 20 days
I.
dSarm Fold Increase

# Fig. 7

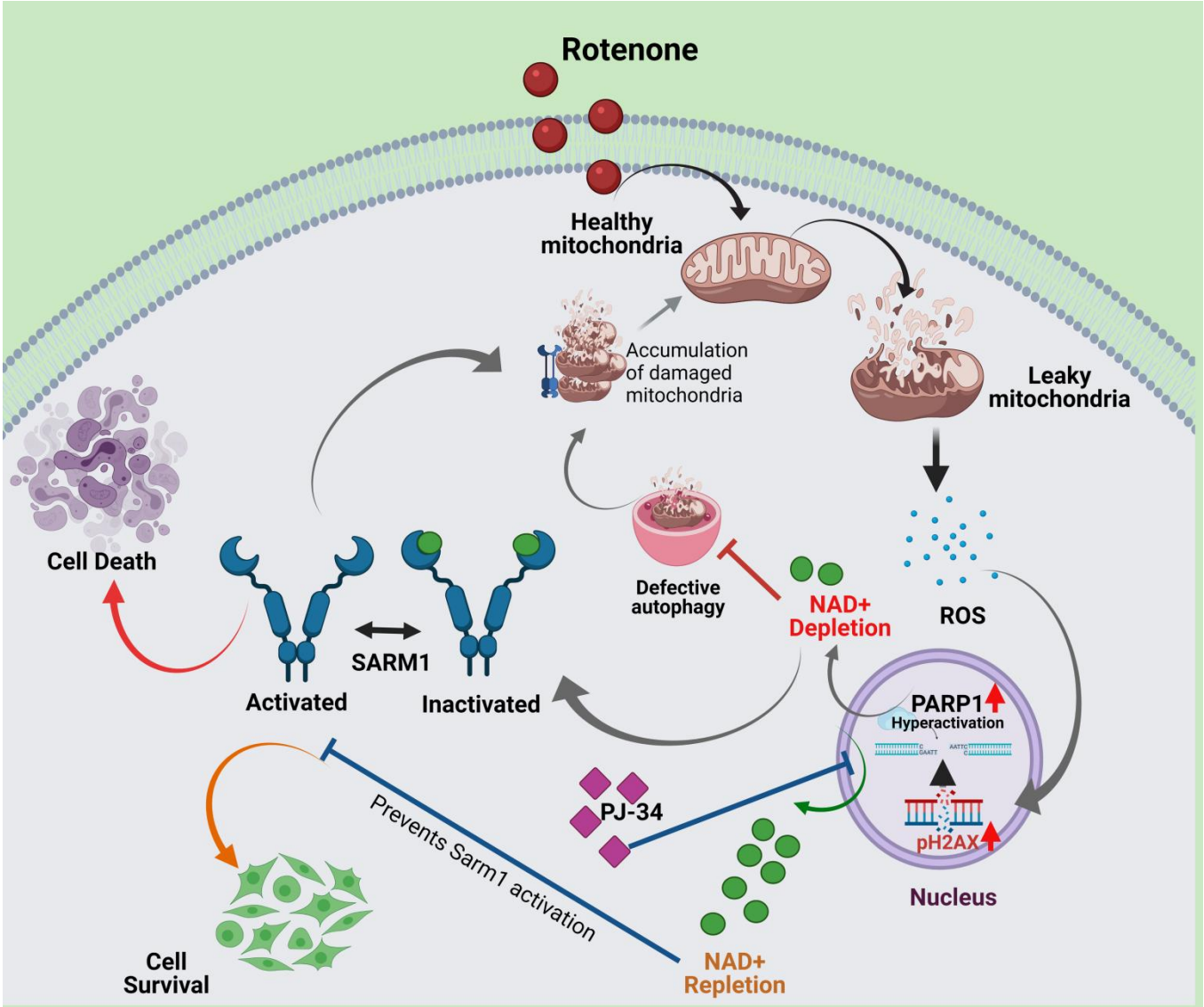
Rotenone
Healthy mitochondria
Accumulation of damaged mitochondria
Leaky mitochondria
Cell Death
Defective autophagy
NAD+ Depletion
ROS
SARM1
Activated
Inactivated
PARP1
Hyperactivation
pH2AX
Nucleus
PJ-34
Prevents Sarm1 activation
Cell Survival
NAD+ Repletion

# Fig. S1

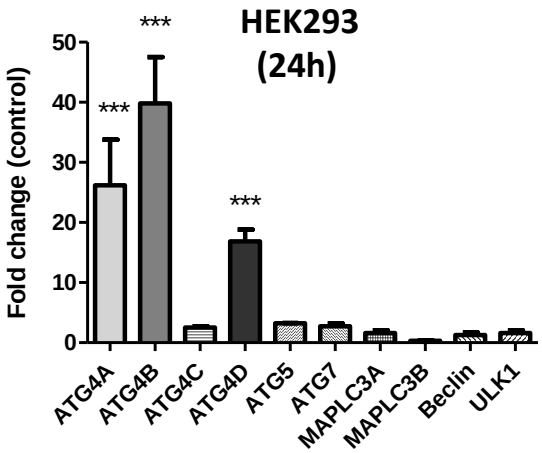
HEK293
(24h)
Fold change (control)
0
10
20
30
40
50
***
***
***
ATG4A
ATG4B
ATG4C
ATG4D
ATG5
ATG7
MAPLC3A
MAPLC3B
Beclin
ULK1

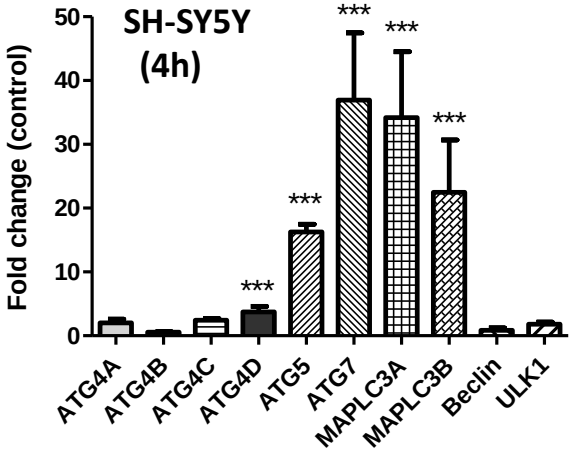
SH-SY5Y
(4h)
Fold change (control)
0
10
20
30
40
50
***
***
***
***
***
***
ATG4A
ATG4B
ATG4C
ATG4D
ATG5
ATG7
MAPLC3A
MAPLC3B
Beclin
ULK1

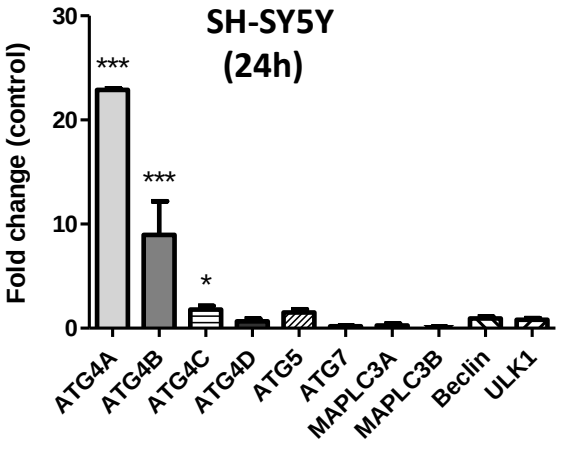
SH-SY5Y
(24h)
Fold change (control)
0
10
20
30
***
***
*
ATG4A
ATG4B
ATG4C
ATG4D
ATG5
ATG7
MAPLC3A
MAPLC3B
Beclin
ULK1

# Fig. S2

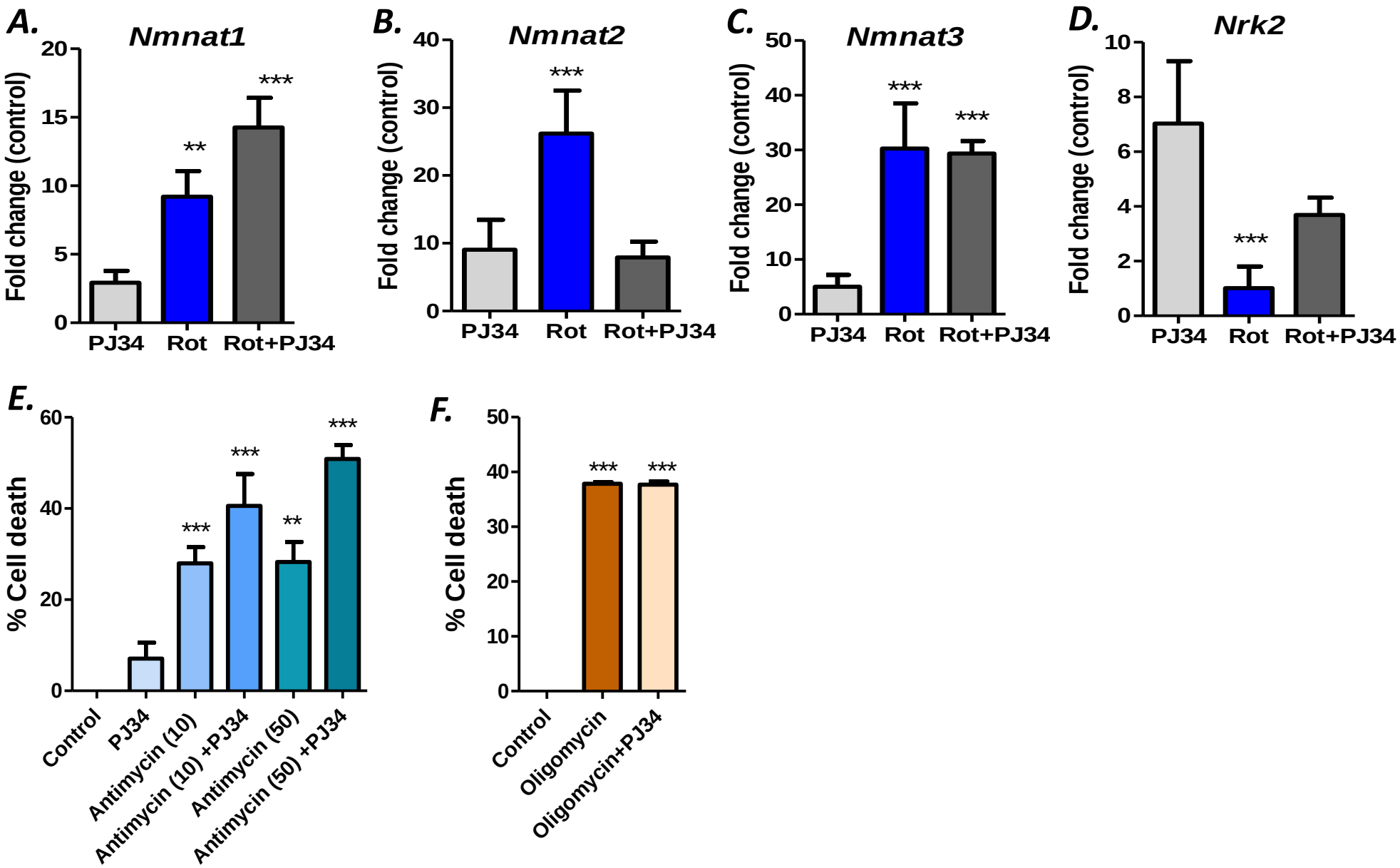
A.
Nmnat1
Fold change (control)
20
15
10
5
0
**
***
PJ34
Rot
Rot+PJ34
B.
Nmnat2
Fold change (control)
40
30
20
10
0
***
PJ34
Rot
Rot+PJ34
C.
Nmnat3
Fold change (control)
50
40
30
20
10
0
***
***
PJ34
Rot
Rot+PJ34
D.
Nrk2
Fold change (control)
10
8
6
4
2
0
***
PJ34
Rot
Rot+PJ34
E.
% Cell death
60
40
20
0
***
***
**
***
Control
PJ34
Antimycin (10)
Antimycin (10) +PJ34
Antimycin (50)
Antimycin (50) +PJ34
F.
% Cell death
50
40
30
20
10
0
***
***
Control
Oligomycin
Oligomycin+PJ34

# Fig. S3

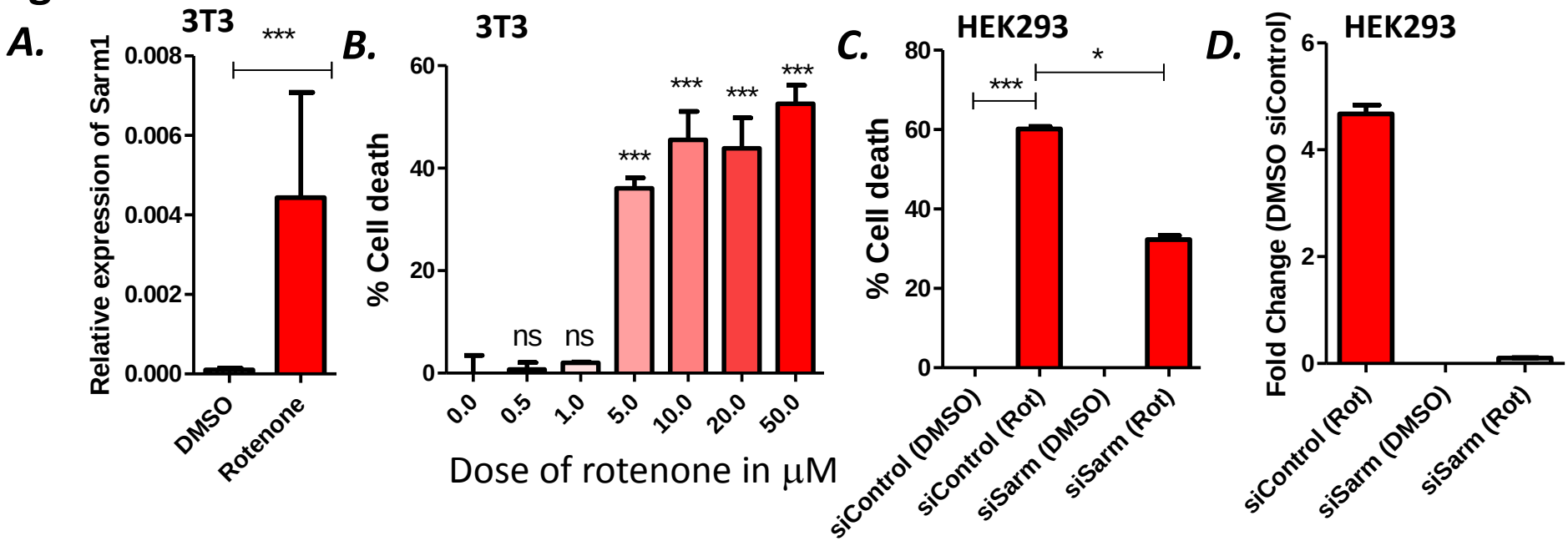
A.
3T3
***
Relative expression of Sarm1
0.008
0.006
0.004
0.002
0.000
DMSO
Rotenone
B.
3T3
% Cell death
60
40
20
0
ns
ns
***
***
***
***
0.0
0.5
1.0
5.0
10.0
20.0
50.0
Dose of rotenone in µM
C.
HEK293
% Cell death
80
60
40
20
0
***
*
siControl (DMSO)
siControl (Rot)
siSarm (DMSO)
siSarm (Rot)
D.
HEK293
Fold Change (DMSO siControl)
6
4
2
0
siControl (Rot)
siSarm (DMSO)
siSarm (Rot)

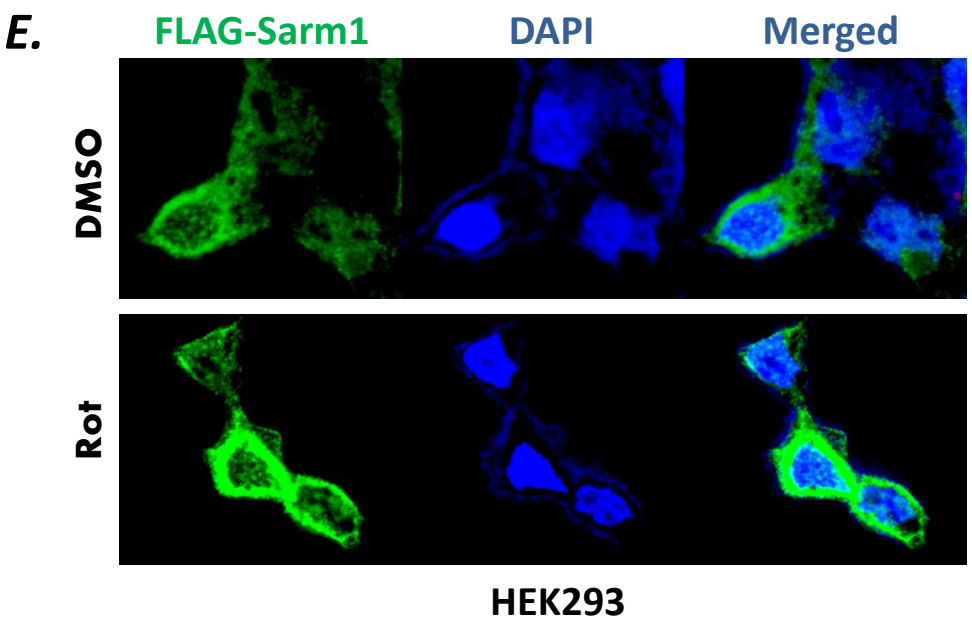
E.
FLAG-Sarm1
DAPI
Merged
DMSO
Rot
HEK293

**Supplementary figure legends**

**Fig. S1. (A-C).** qRT-PCR analysis of the fold change in gene expression of selected autophagy genes at 4 or 24 h post rotenone treatment in HEK293 (A) and SH-SY5Y (B-C) cells with respect to DMSO treated controls. Gapdh was used as an internal control for the analysis.

**Fig. S2. (A-D).** qRT-PCR analysis of the fold change in gene expression of Nmnat1 (A), Nmnat2 (B), Nmnat3 (C) and Nrk1 (D) at 24 h post rotenone treatment in HEK293 with respect to DMSO treated controls. Gapdh was used as an internal control for the analysis **(E-F)** Cell viability assay in HEK293 cells pre-incubated with 25 µM PJ-34 for 1 h followed by treatment with the mitochondrial complex III inhibitor Antimycin A (10 µM and 50 µM) (E) and the mitochondria complex V inhibitor Oligomycin (500nM) (F). The percentage of cell death was determined by the $OD_{540}$ values in an MTT assay.

**Fig. S3. (A).** qRT-PCR analysis of Sarm1 gene expression at 24 h post rotenone treatment in 3T3 cells. Gapdh was used as an internal control **(B).** MTT assay of cells treated with indicated doses of rotenone at 24 h post treatment in 3T3 cells **(C).** Cell viability assay in Sarm1 knock-down HEK293 cells followed by rotenone treatment for 24 h and the results were compared with control siRNA samples. **(D)** qRT-PCR analysis of the fold change in gene expression of Sarm1 at 24 h post rotenone treatment in HEK293 with respect to DMSO treated controls in both siControl and siSarm1 samples. Gapdh was used as an internal control for the analysis. Data are representative of two independent experiments with three replicates per sample **(E).** Immunofluorescence analysis of HEK293 cells transfected with FLAG-tagged full length Sarm1 (Green) for 48 h followed by rotenone (500 nM) treatment for 24 h. Results were compared with DMSO treated but transfected cells. Nuclear staining is represented with DAPI (blue).

## Supplementary Table1:

| Name of the Gene | Forward Sequence (5'-3') | Reverse Sequence (5'-3') |
|---|---|---|
| **hGapdh** | GCCTTCTCCATGGTGGTGAAGAC | CCCATCACCATCTTCCAGGAGC |
| **hSarm1** | GCTTGAACATGTGCTCCAAGATGCC | GAGCAGATCCTGGTGGCTGAGAA |
| **Atg4A** | CCTGGGACTTGTAGTTCTGCACTG | GTTTGAGAGCAGTTCCGGGCA |
| **Atg4B** | GTAGCTGCGTCCATCTTCCCAG | CGGCACACCTATTGGCCCB |
| **Atg 4C** | CACGCAGACGTTCCGACC | TCTTACTACGGTGGCCGGG |
| **Atg 4D** | ACACTGAGTTCATGGACGCGC | TAAGATGGCGATGGCTGCGG |
| **Atg 5** | CTGTCATTTTGCAATCCCATCCAGAGTTG | CTTCTGCACTGTCCATCTAAGGATGC |
| **Atg 7** | CTGCAGTTTAGAGAGTCCAGGATCCC | CAGAGAGAGCTGTGGTTGCCG |
| **Maplc3A** | GTGTCTGCGGTTTGGGGG | TCACCGGGCGAGTTACCTC |
| **Maplc3B** | CGGCATGGTGCAGGGATC | TGAGGAGATACAAGGGAAGTGGCT |
| **Becn1** | GAGCGAGGCCTCCAGAACTAC | AGCGTCACGTCCGGTCTC |
| **Ulk1** | CCCTTGAAGACCACCGCG | AGAGACCGTGGGCAAGTTCG |
| **Nmnat1** | GCCAGTCCCAGAGTTTAGGG | GACTCCACCACACCATCCTG |
| **Nmnat2** | ATGACGAGACCACCAAGAC | CTAGCCGGAGGCATTGATGT |
| **Nmnat3** | ATGAAGAGCCGAATACCTGTG | CTATGTCTTGCCCTCAG |
| **Nrk2** | AGGATGACTTCTTCAAGCCCC | GGAGGATGTGGGTGTCCGAG |
| **dGapdh** | TTGATGTTGGCCGGGTCGC | GTGGCCGTCAACGATCCCTTC |
| **dSarm** | AAGGGAGCCCTCTCACTCCGC | ACTTTGCACCGTAATACTGGAGGC |